Interactions of helices on interdomain interface couple the chemistry of intermediate formation with allostery in *Plasmodium falciparum* GMP synthetase

Santosh Shivakumaraswamy[1], Nivedita Pandey[1], Lionel Ballut[2], Sébastien Violot[2], Nushin Aghajari[2], Hemalatha Balaram[1*]

[1]Molecular Biology and Genetics Unit, Jawaharlal Nehru Centre for Advanced Scientific Research, Bengaluru, Karnataka 560064, India.

[2]Biocrystallography and Structural Biology of Therapeutic Targets, Molecular Microbiology and Structural Biochemistry, UMR 5086, CNRS, University of Lyon 1, 7 passage du Vercors, 69367 Lyon Cedex 07, France.

[*]To whom correspondence should be addressed: Hemalatha Balaram, Molecular Biology and Genetics Unit, Jawaharlal Nehru Centre for Advanced Scientific Research, Bengaluru, Karnataka 560064, India; hb@jncasr.ac.in; Tel. +91-80-22082812; Fax +91-80-22082766.

Abstract

GMP synthetase, a member of the glutamine amidotransferase family of enzymes catalyses the substitution of the C2 oxo-group of the purine base in XMP with an amino-group generating GMP, the last step in the biosynthesis of GMP. This seemingly simple reaction involves a complex series of catalytic events that include hydrolysis of the side chain of Gln generating ammonia in the glutamine amidotransferase domain (GATase), activation of XMP through generation of adenyl-XMP intermediate in the ATP pyrophosphatase domain (ATPPase) and tunnelling of ammonia from the GATase to the ATPPase domain where it reacts with the intermediate generating GMP. The catalytic events across the two domains are highly coordinated, resulting in an enzymatic machinery that functions without wastage of either ATP or Gln. Herein, we have taken recourse to the analysis of structures and sequences of GMP synthetases, site-directed mutagenesis and enzymatic assays on the *Plasmodium falciparum* enzyme to decipher the molecular basis of domain coordination. Our studies show that residues on three helices at the domain interface are crucial for interdomain crosstalk. Further, we show that residues on these helices along with those on a loop referred to as lid-loop, play essential roles in catalysing adenyl-XMP formation. By way of intricately connecting residues involved in domain crosstalk with catalysis in ATPPase domain, the two domains in *P. falciparum* GMP synthetase synchronize their catalytic events. These results add significantly to our understanding of the working of GMP synthetases, which are drug targets in many infectious pathogens.

Keywords: *Plasmodium falciparum,* glutamine amidotransferase, GMP synthetase, domain crosstalk, allostery

Abbreviations: GATase, glutamine amidotransferase; ATPPase, ATP pyrophosphatase; GATs, glutamine amidotransferases; GMPS, GMP synthetase; PfGMPS, *Plasmodium*

falciparum GMP synthetase; WT, wild type; EcGMPS, *Escherichia coli* GMP synthetase; SEM, standard error of the mean

Introduction

Glutamine amidotransferases (GATs) are enzymes that operate in different biosynthetic pathways where they catalyse the replacement of an oxo group with an amino group. To achieve this chemical change, GATs have evolved as enzymes with modular catalytic units with each unit comprised of a domain or subunit catalysing a specific reaction [1–3]. In general, the reaction catalysed by GATs involves the hydrolysis of the amide side chain of Gln by the glutamine amidotransferase (GATase) domain generating ammonia followed by amination of the acceptor molecule in the acceptor domain. The latter reaction is often facilitated by the formation of a metastable adenylated/phosphorylated intermediate using ATP as the adenyl/phosphate donor. The ammonia generated by Gln hydrolysis is tunnelled to the acceptor domain where it attacks the activated acceptor leading to the formation of the aminated product [4–6]. Despite the evolution of a tunnelling mechanism, *in vitro* assays have shown that most GATs also utilize externally available ammonia, a reaction that may not be physiologically relevant [1,2]. The catalytic events occurring in the two domains are coordinated to ensure product formation and that the utilization of neither Gln nor ATP is futile. Moreover, hydrolysis of Gln is under stringent regulation as the GATase is active only when the acceptor domain is primed to receive ammonia [3,7,8]. A design involving intricate organization of the two domains enables allosteric activation of the GATase domain, coordination of the catalytic events and ammonia tunnelling in all GATs. The reactions catalysed by GATs are indispensable for various cellular functions, and hence, many GATs are being pursued as drug targets against cancer, infectious pathogens and towards development of herbicides [9–13].

GATs are classified largely into class I or II based on the fold of the GATase domain [14]. The GATase domain in class I or triad GATs consists of an α/β hydrolase fold and a catalytic triad of Cys, His and Glu residues [15]. Among the nine triad GATs reported till date, crystal structures for eight enzymes are available [16–24]. From these structures, it is clear that variations in ammonia tunnelling mechanisms exist. Whereas, preformed conduits for tunnelling ammonia are seen in some, in other cases tunnel is evident upon substrate binding [7,9,20]. Examples of triad GATs in whose structures a tunnel cannot be visualized are also present [25]. 2-amino-2-desoxyisochorismate synthase and CTP synthetase are triad GATs that show a difference in the relative orientation of the two domains upon ligand binding [20,26]. In most of the available crystal structures of GMP synthetase (GMPS), another triad GAT, the catalytic pocket in the acceptor and GATase domains are exposed to the aqueous environment (Fig. 1a). Also, the crystal structures do not reveal an ammonia tunnel connecting the two active sites [22,27]. Regardless of the distal arrangement of active sites and the absence of a tunnel, biochemical studies provide evidence for regulation of GATase activity by the binding of substrates to the acceptor domain and ammonia tunnelling [28,29]. Our recent crystal structure of *P. falciparum* GMPS (PfGMPS) has revealed that an 85° rotation of the GATase domain (Fig. 1b) underlies coupling of activity across the two catalytic pockets and ammonia tunnelling [30].

The functioning of PfGMPS has been addressed by biochemical experiments and crystal structures [28–30]. The enzyme catalyses the conversion of XMP to GMP with the catalytic event in the acceptor domain (ATP pyrophosphatase domain (ATPPase)) being the synthesis of adenyl-XMP intermediate from ATP.Mg^{2+} and XMP (Fig. 2). The ammonia generated in the GATase domain by the hydrolysis of Gln is tunnelled to the ATPPase domain where it attacks the adenyl-XMP intermediate generating GMP [29]. Unlike other GMP synthetases, PfGMPS is unique in displaying a basal GATase activity even when

substrates are not bound to the ATPPase domain [28]. The binding of substrates to the ATPPase domain creates a high-affinity Gln-binding pocket leading to a lowering of the $K_{m(app)}$ value for Gln by 360-fold along with upregulation of GATase activity by 8-12 fold [30]. Apart from information flow from the ATPPase towards the GATase domain, the inhibition of ammonia dependent GMP formation by Gln binding to a GATase inactive PfGMPS_C89A mutant suggests bidirectional interdomain crosstalk in PfGMPS [29]. Using the 85° GATase domain-rotated structure, the path traversed in achieving this domain reorganization was reconstructed. This revealed that coupling of the active sites through a tunnel is possible at an intermediate state of GATase rotation, thus resolving the mechanism of ammonia transfer [30].

Despite these studies, a comprehensive understanding of the molecular mechanism of GATase activation as well as the coordination of the two active site chemistries is lacking in GMP synthetases. Towards this end, we analyzed the sequence and structural motifs at the GATase-ATPPase interface across all available structures of GMP synthetases and validated our observations by performing assays on site-directed mutants of PfGMPS, which reported on the activity of the individual domains as well as GMP formation. Further, by identifying residues in the ATPPase domain involved in catalysing the formation of adenyl-XMP intermediate and tracing their connectivity with residues that mediate domain crosstalk, we present the molecular basis of active site synchronization for the first time. We have also attempted to understand the functional implications of the obligate dimeric nature of GMP synthetases from prokaryotes and parasitic protozoa, including PfGMPS, a feature distinct from most eukaryotic homologs that are monomers.

Results and discussion

Crystal structures of PfGMPS and other available GMP synthetases were examined to identify residues involved in domain crosstalk and catalysis in the ATPPase pocket. The

findings from the analysis of the structures and sequence conservation are detailed in the section below. These observations were validated by generating eighteen site-directed mutants of PfGMPS and subjecting them to a series of enzymatic assays. The mutants of PfGMPS were expressed in *Escherichia coli* and purified to greater than 95% homogeneity (Fig. S1). The lack of any significant difference in the far-UV circular dichroism spectra of the wild type (WT) and mutants confirmed that the overall secondary structure was largely retained (Fig. S1). Further, similar to PfGMPS, the mutants were dimers on size-exclusion chromatography, indicating no significant perturbation in quaternary assembly (Fig. S1). The mutants were then subjected to enzymatic assays to assign the role of the mutated residue to one or more steps in the catalytic conversion of XMP to GMP. The enzymatic function of GMPS can be split into three key steps; adenyl-XMP formation in the ATPPase domain, activation of GATase domain to enable Gln hydrolysis and GMP synthesis using either Gln or NH_4Cl as nitrogen source with the former entailing ammonia tunnelling (Fig. S1). The kinetic parameters for GMP synthesis for the WT and mutant enzymes were determined by steady-state assays using Gln and NH_4Cl as the nitrogen source. The rate (*k*') of adenyl-XMP formation was measured with ATP.Mg^{2+} and XMP as substrates using a stopped-flow spectrophotometer, in the absence of an ammonia source. The formation of the intermediate results in a single-phase exponential drop in absorbance at 290 nm and the derived value of the exponential phase rate constant, *k*' reports on the ability of the enzyme to synthesize the intermediate. The enhanced rates of hydrolysis of Gln due to allosteric activation of the GATase domain by the binding of substrates to the ATPPase domain were measured using L-glutamate dehydrogenase as the coupling enzyme to detect the liberated glutamate. As activation of glutaminase domain is a measure of ligand binding to the ATPPase domain, we have used this coupled enzyme assay to determine ATP.Mg^{2+} and XMP binding affinities (K_d

values) of mutants that are inactive in GMP formation but showed at least 40% GATase activation. The results of these experiments are discussed in the following sections.

Highly conserved salt bridges are part of interdomain interface in GMPS

Residues that could be involved in domain crosstalk were identified by examining the GATase-ATPPase interface in the nine available GMPS structures and scored for their conservation across GMPS sequences from diverse species covering eukaryotes and prokaryotes (Fig. S2). The GATase-ATPPase domain orientation is similar in all GMPS structures except in the Gln-complexed PfGMPS_C89A structure. We refer to the state of the domain rotation in PfGMPS_C89A_Gln complex as the 85° and the others as 0° (Fig. 1). The interdomain interface in the 0° GMPS structures is predominantly composed of the N-terminal helix, α1 of the GATase domain and helices α11 and α12 of the ATPPase domain (Fig. 3a, b). Alignment of GMPS sequences reveals that the three helices harbour conserved motifs with (K/R)(K/R)XRE (α1 motif), DXXES (α11 motif) and KD(D/E)V(K/R) (α12 motif) being the signature motifs (Fig. 3a). The charged residues in the 4th and 5th positions of the α1 motif are replaced with Asn in sequences from *Plasmodium* species. Further, the conserved D/E and K/R substitutions in the α12 motif are limited to sequences from *Plasmodium* (Fig. S2).

The α1-α12 interdomain interactions are largely conserved in all 0° structures of GMPS. The first and the fourth residues of α1 motif ((K/R)(K/R)XRE) form two interdomain salt bridges with the second and third residues of the α12 motif (KD(D/E)V(K/R), respectively, though in *Neisseria gonorrhoeae* GMPS the distance between the interacting pairs is above 4 Å (Table S1). In PfGMPS (PDB ID 3UOW, 4WIM), due to disorder of the side chains, interdomain salt bridges are not directly evident. However, through modelling of missing side chains or structural superposition of protomers from the two structures (3UOW and 4WIM), the atoms involved in salt bridge formation between Lys24 (α1) and

Asp412/Asp413 (α12) come within a distance of ≤ 4 Å (Fig. 3c and Table S1). The second salt bridge is absent in PfGMPS as the fourth residue of the α1 motif is an asparagine. Unlike α12, the residues of α11 across the GMPS structures, show varying levels of disorder indicating conformational flexibility of this segment. Also, an interdomain salt bridge involving His20 preceding the α1 motif and Glu374 of α11 motif was observed by superposing two chains of PfGMPS (Fig. 3c) [30]. His20 is not conserved across GMPS sequences (Fig. S2) and this salt bridge is absent in all other GMPS structures except in *Neisseria gonorrhoeae* GMPS where the histidyl residue is replaced by Arg (Table S1 and Fig. 3a, c). Other interdomain salt bridges are enzyme-specific and the interacting residues are not conserved.

In the PfGMPS_C89A/Gln structure (PDB ID 4WIO), on account of GATase rotation, a different set of GATase residues interact with residues on α11 and α12 (Fig. 3d). Whereas the side chains of many residues constituting this 85° interface are disordered, an examination of the structure shows that the side chains of the residue pairs Glu213/Lys376 and Lys160/Asp412 could be involved in forming interdomain salt bridges (Fig. 3e). It should be noted that while Lys376, a non-conserved residue follows the α11 motif, Asp412 that is invariant is part of the α12 motif. Residues Glu213 and Lys160 are in the GATase domain (Fig. 3a) and are not conserved (Fig. S2).

Interdomain interactions in the 0° interface modulate allostery and domain crosstalk

The significance of α1-α12 interactions was investigated in PfGMPS by mutating Lys24 of the α1 motif in the GATase domain and Asp412 as well as Asp413 of the α12 motif in the ATPPase domain. Compared to WT, the mutants K24L, D412A and D413A of PfGMPS showed a common increase in $K_{m(app)}$ value for the substrate glutamine with PfGMPS_D412A showing the highest (7.9-fold) increase. Regarding k_{cat}, while PfGMPS_K24L showed a drop for Gln (2.6-fold) and NH_4Cl (2.3-fold) dependent GMP formation, the values for D412A and

D413A mutants of PfGMPS remained unaltered from that of the WT (Table 1). The levels of GATase activation by the binding of ligands to the ATPPase domain were reduced by 1.5 to 1.8-fold in the three mutants while the values of *k*' (rate constant for the formation of adenyl-XMP) were not significantly altered in the PfGMPS mutants K24L and D413A. PfGMPS_D412A showed a 1.4-fold increase in *k*' (Fig. 4).

Earlier studies have shown that mutation of His20 on α1 impairs enzyme function [30]. Here we show that mutation of Lys24 (α1) or the interacting partners Asp412/Asp413 (α12) results in a reduction in the affinity of the enzyme for Gln. Since GATase activation is enabled by an increase in the affinity of the enzyme for Gln, the increase in $K_{m(app)}$ value for Gln observed upon disrupting the α1-α12 interactions shows the importance of this interdomain crosstalk in GATase activation. Similar to our previous study on PfGMPS_H20A [30], mutation of Lys24 (α1) also resulted in a reduction in turnover of both Gln and NH_4Cl dependent GMP formation. The impairment of even NH_4Cl dependent GMP formation highlights the importance of GATase residues in the activity of the ATPPase domain. These results suggest that the two modules have evolved as a single entity to optimize the Gln dependent reaction, which necessitates the coordination of Gln hydrolysis and adenyl-XMP formation. The involvement of α1 in domain crosstalk is supported by experiments on two-subunit type GMPS from *Methanocaldococcus jannaschii* where the binding of substrate-bound ATPPase subunit induced chemical shift changes in residues on helix α1 as well as the loops containing the catalytic triad of the GATase subunit [31].

Interdomain interactions in the 85° interface also modulate allostery and domain crosstalk

One of the GATase-ATPPase interdomain salt bridge in the 85° rotated structure of PfGMPS is between Glu213 on a GATase loop and Lys376 on helix α11 (Fig. 3e). The loop containing Glu213 also harbours His208 and Glu210, two of the catalytic triad residues. Although

mutation of Glu213 to Ala and Lys376 to Leu affected the turnover of Gln and NH_4Cl dependent GMP formation only marginally, the $K_{m(app)}$ value for Gln was increased by 3.9 and 4.4-fold for the E213A and K376L PfGMPS mutants, respectively (Table 1). The GATase activation and *k*' for adenyl-XMP formation were significantly lower in PfGMPS_E213A mutant, however, the changes in K376L were insignificant (Fig. 4). The second interdomain salt bridge in the 85° interface is between Asp412 of the α12 motif and Lys160 on the GATase domain. Mutation of Lys160 to Leu did not affect the kinetic parameters (Table 1) nor the levels of GATase activation or the *k'* for adenyl-XMP formation (Fig. 4). However, as discussed above, mutation of Asp412, which is also involved in interdomain salt bridges in the 0° interface, impairs allosteric activation of the GATase domain.

In the two available 0° PfGMPS structures (PDB IDs 3UOW, 4WIM), the side chain of Glu213 that is ordered in two out of the four chains does not interact with the side chain of Lys376 and is at a distance of 26 Å. Hence, the interdomain interactions between Glu213 and Lys376 become evident only in the GATase rotated state (Fig. 3e). The impaired affinity for Gln upon mutation of Glu213 and Lys376 and the drop in *k*' value for adenyl-XMP formation from 184 ± 4 min^{-1} to 109 ± 6 min^{-1} in case of the PfGMPS_E213A mutant validates that the rotation of the GATase domain and interactions in the 85° rotated state are integral to allostery and catalysis in the ATPPase domain. Also, corroborating these observations is a study in which through modelling, the GATase active site was placed against the ATPPase active site in *E. coli* GMPS (EcGMPS). In this structure, the EcGMPS residue His186 (analogous to Glu213 in PfGMPS) forms an interdomain salt bridge with Glu383 on α12. Mutation of His186 to Ala resulted in an increase in the K_m value for Gln by 50-fold and uncoupling of the two reactions [32]

Interface helix residues of the ATPPase domain are also involved in catalysis

Residues Arg25 on α1, Asp371 on α11, and Lys411 and Lys415 on α12 are either invariant or conservatively replaced but have side chains directed away from the interdomain interface (Fig. 3a and 5). Mutation of Arg25, the second residue of the α1 motif to Leu did not result in any significant change in kinetic properties (Table 1). The level of GATase activation was marginally higher than WT and the *k*' for adenyl-XMP formation remained unchanged (Fig. 4). The almost complete impairment of adenyl-XMP formation upon mutation of Asp371 to Ala in PfGMPS, reported in our previous study, indicates a key catalytic role for this residue on the interface helix α11 [30]. Similarly, mutation of Lys411 on helix α12 to Leu resulted in a complete loss of Gln and NH_4Cl dependent GMP formation, arising from the complete absence of adenyl-XMP formation in stopped-flow assays (Fig. 4). However, unlike in PfGMPS_D371A where GATase activation was higher than WT [30], the 70% drop seen in PfGMPS_K411L indicates that substrate(s) binding is highly compromised. Mutation of Lys415 to Leu did not significantly alter the steady-state kinetic parameters for Gln and NH_4Cl dependent GMP formation except the $K_{m(app)}$ value for ATP that was 4.2-fold higher compared to WT and this is reflected in the *k*' for adenyl-XMP being lower by 2.7-fold (Table 1 and Fig. 4). The activation of GATase domain was modestly higher compared to WT (Fig. 4).

The structures of PfGMPS throw light on the possible roles of Asp371 (α11) and Lys411 (α12) in substrate binding and catalysis of adenyl-XMP formation. Superposition of AMP and PPi from the EcGMPS structure (PDB ID 1GPM) on XMP complexed PfGMPS structure (PDB ID 3UOW) shows that the side chain of Asp371 is placed above the expected location of the adenyl-XMP bond at 6.7 Å from C2 oxygen of xanthine while Lys411 forms a salt bridge with the phosphate of PPi that is distal to AMP (corresponding to γ-phosphate of ATP) (Fig. 5b). The helix α11 is tilted into the active site in the Gln bound PfGMPS_C89A

structure and a further movement of α11 could bring the side chain atoms of Asp371 into interacting distance with the α-phosphate of ATP that is involved in adenyl-XMP formation. The structural observation of Lys411-PPi interaction is validated by the large drop seen in GATase activation in PfGMPS_K411L. The highly conserved Lys415 also plays a role in ATP binding as evident from the 4.2-fold increase in $K_{m(app)}$ value for this substrate in PfGMPS_K415L. Although the ζ-amino group of this residue in the PfGMPS structures (PDB IDs 3UOW, 4WIM) is devoid of contacts with ligand or with other residues (Fig. 5b), in most other GMPS structures the side chain of this residue is involved in H-bonding interactions with main chain atoms of residues lining the ATPPase pocket. This suggests an indirect role for Lys415 in ATP binding.

The lid-loop invariant residues are crucial for adenyl-XMP formation

Apart from Asp371 and Lys411 on the interdomain helices α11 and α12, that protrude into the active site and impact adenyl-XMP formation, the 85° rotated PfGMPS_C89A/Gln structure for the first time provides a comprehensive picture of the ATPPase active site and enables the identification of other residues involved in catalysis [30]. In all the 0° structures of GMP synthetases, a 25-residue long loop connecting α11 with β12, termed the lid-loop, is disordered except in human GMPS where the loop is mapped but away from the ATPPase active site. However, in the PfGMPS_C89A/Gln structure, except for eight intervening residues, the remaining residues of the lid-loop are mapped and positioned in the ATPPase active site (Fig. 6a). The lid-loop has an invariant motif IK(T/S)HHN (residues 385-390 in PfGMPS) and the side chain nitrogen atoms of Lys386, His388 and His389 from the motif are within 4 Å of AMP phosphate (superposed from EcGMPS) (Fig. 6b and S2).

The residues KTHHN of the invariant motif were mutated to examine their role in adenyl-XMP formation. The mutants of PfGMPS, K386L, H388A and H389A showed very weak activity ranging from 65-fold to 731-fold drop compared to WT for both Gln and

NH_4Cl dependent GMP formation (Table 2). Stopped-flow experiments revealed that the rate of adenyl-XMP formation in PfGMPS_H388A was 24-fold lower than WT while the *k*' values could not be estimated for the mutants PfGMPS_K386L and PfGMPS_H389A as the change in absorbance at 290 nm was below sensitivity of detection (Fig. 6c). Whereas the levels of GATase activation in H388A and H389A mutants of PfGMPS were 51 and 43% of the WT, respectively, PfGMPS_K386L showed a large drop to 19 % that is only marginally greater than background basal (without binding of ATP.Mg^{2+} and XMP) glutaminase activity of PfGMPS (Fig. 4). The K_d values for the complex of PfGMPS mutants H388A and H389A with ATP.Mg^{2+} and XMP are in the low micromolar range (Table S2) while the low level of activation in PfGMPS_K386L precluded K_d measurement. These results indicate that Lys386 like Lys411, is essential for the binding of ATP.Mg^{2+} and XMP, whereas His388 and His389 are involved in the synthesis of the adenyl-XMP intermediate. With just a minor reduction, the specific activity of Gln and NH_4Cl dependent GMP formation for the PfGMPS_T387A mutant was comparable to WT while PfGMPS_N390A was completely inactive. However, both the mutants could synthesize the adenyl-XMP intermediate albeit at reduced rates as the $k^{'}$ for adenyl-XMP formation was 3-fold and 7-fold lower in the T387A and N390A mutants of PfGMPS, respectively (Fig. 4 and Fig. 6c). The activation of the GATase domain in PfGMPS_T87A was reduced by 23% while it was enhanced to 200% of WT in PfGMPS_N390A (Fig. 4).

The increase in electrophilicity of C2 of XMP enabled through the formation of the unstable adenyl-XMP intermediate facilitates attack by ammonia and thereby the replacement of the C2 oxygen with nitrogen. Transfer of AMP from ATP to XMP is an adenylation reaction that is facilitated by the ATP α-phosphorous undergoing geometric as well as electrostatic changes involving the development of strong negative charges on the non-bridging oxygen atoms in the transition state [33,34]. Since stabilization of transition state

underlies enzymatic rate enhancements, all phosphoryl transfer enzymes, including adenylating enzymes, employ positively charged groups to interact with and neutralize the negative charges on the non-bridging oxygen atoms [35]. The above results suggest a dominant role for His389 and also a possible function for His388 in the stabilization of the transition state as both H388/389A mutants of PfGMPS bind ATP.Mg^{2+} and XMP, but are highly or completely impaired in adenyl-XMP formation.

In the adenylating enzyme tyrosyl-tRNA synthetase, the KSMKS loop changes its conformation from an open to a closed-form upon binding ATP. This closure results in a movement of the ζ-amino group of Lys235 (KSMKS motif) close to the ATP α-phosphate thereby resulting in catalysis [36,37]. The results with the PfGMPS lid-loop mutants suggest that even in GMP synthetases, binding of ATP.Mg^{2+} and XMP induces conformational changes in the lid-loop culminating in the repositioning of the IK(T/S)HHN motif residues into proximity with the ATP α-phosphate, facilitating transition state stabilization.

With regard to the invariant asparaginyl residue in the lid-loop motif, the 7-fold drop in *k*' in PfGMPS_N390A suggests an indirect role for this residue possibly arising from loss of H-bonding interactions that in turn could perturb the conformation of His388 and His389, residues that stabilize the transition state. The complete absence of GMP formation in this mutant strongly indicates a role for this residue in facilitating the chemistry involving the reaction of NH_3 with adenyl-XMP.

Conserved C-terminal residues from both protomers are involved in XMP binding

The C-terminus of GMP synthetases contains a 13-residue long loop with the highly conserved signature motif KPPXTXE(F/W)X (residues 547-555 in PfGMPS) at its end (Fig. 3a and S2). The ζ-amino group of Lys547 interacts with the phosphate of XMP (Fig. 7a). The peptide bonds Lys547-Pro548-Pro549 are in the cis configuration, which, induces a turn in the polypeptide chain and enables the interaction of Glu553 carboxy with ribose 2' hydroxy

group. In addition, the α-carboxy of the terminal Glu555 residue forms a salt bridge with guanidino group of Arg336 that in turn interacts with C6 oxygen and the N7 of XMP (Fig. 7a). Hence, the residues of the C-terminal loop make direct and indirect contacts with XMP. The conformation of the loop is also restrained by dimer interactions involving H-bonds between the Nη2 of Arg539' (from the neighbouring chain) and backbone CO of both Thr551 and Glu553 (Fig. 7b).

We probed the role of C-terminal loop residues Lys547, Glu553, Glu555 as well as the importance of the interdimer interactions of Arg539 by mutating them to Leu. The K547L, E553L and R539L mutants of PfGMPS were inactive for Gln and NH_4Cl dependent GMP formation while the activity of PfGMPS_E555L was only marginally lower than WT. The levels of GATase activation in the inactive mutants were 22-26% of the WT and stopped-flow assays revealed that these mutants are inactive for adenyl-XMP formation (Fig. 4). The GATase activation in E555L mutant was however similar to WT and the *k*' for adenyl-XMP synthesis was 1.6-fold lower.

The low levels of GATase activation in PfGMPS mutants R539L, K547L and E553L suggest that ligand binding is weak, which is supported by the complete absence of activity for GMP synthesis even when NH_4Cl is used as a source of ammonia. The results validate the crystallographic observations of the interactions of the side chains of these residues with XMP and highlight their critical role in binding this ligand. The results of the E555L mutant indicate that the interactions of the side chain of the terminal Glu residue are unimportant. The fact that the main chain carboxylate of Glu555 forms a salt bridge with the XMP-interacting Arg336, suggests that any residue may occupy the C-terminal position and this is supported by the non-conserved nature of this residue. The lack of activity of the R539L mutant proves that the interdimer interactions are indispensable for PfGMPS catalysis. Unlike human GMPS and GMPS from higher eukaryotes which possess a 150 residue insertion in

the dimerization domain that allows them to function as monomers, GMP synthetases from prokaryotes and certain eukaryotes including *P. falciparum* are obligate dimers [28,38–41]. The contribution of residues from the neighbouring monomer in substrate binding and catalysis reveals a significant difference in the ATPPase active site of pathogens and the human host. This difference in the ATPPase active site could be exploited in the design of inhibitors targeting GMP synthetases from *P. falciparum* and other pathogens.

Conclusions

Although nitrogen is one of the abundant elements in an organism, the incorporation of nitrogen into metabolites is not straight forward since this requires the production of a reactive nitrogen atom (with its lone pair of electrons) as well as activation of the metabolite that is to be aminated. In order to exchange as well as sequester ammonia, and protect the activated acceptor, GATs have evolved a design where the two domains are highly intertwined. Although GMP synthetases display an arrangement where the connection between the active sites of the two domains is not readily evident, an 85° rotation of the GATase domain enables the transfer of ammonia. However, the mechanism of interdomain crosstalk leading to GATase activation and coordination of catalytic events was unclear and the investigations reported in this article shed light on these aspects.

The interdomain interactions of many residues residing in the interface helices, α1 of GATase and α11 and α12 of ATPPase, are essential for domain crosstalk. Mutation of these residues impairs allostery, thus establishing that the interface helices are conduits for information exchange. While residues that are involved in interdomain interaction whose mutation impairs allostery are on one face of the helices, the residues on the other face point at the interior of the respective domains. Such residues on ATPPase helices α11 and α12 and the residues on the lid-loop which follows α11, play roles in either substrate binding (α12: Lys411, lid-loop: Lys386) or in catalysing adenyl-XMP formation (α11: Asp371, Glu374,

lid-loop: His388, His389). This establishes that residues on helices α11 and α12 can relay the state of substrate occupancy and/or the formation of adenyl-XMP intermediate to the residues on GATase helix α1. Although mutation of residues Tyr18 [30] and Arg25 that are at either end of helix α1 did not affect catalytic properties, examination of the structure shows connectivity that extends from α1 into the GATase active site. Many residues on α1 pointing into the GATase active site are within 4 Å from residues on the loop harbouring the catalytic His208 and Glu210 (Fig. 5a). By way of tracing the connectivity of the ATPPase catalytic pocket to the GATase catalytic pocket, these results explain the molecular basis of GATase activation (Fig. 8). GMP synthetases thus display an ingenious design of placing helices at the domain interface where residues on one face of the helices catalyse adenyl-XMP formation whereas those on the other face interact with the GATase domain and modulate the affinity of this domain for Gln. This permits coupling the events in ATPPase domain (ATP/XMP binding and adenyl-XMP intermediate formation) with GATase activation leading to the coordination of the catalytic events across the two domains.

The lid-loop augments these processes since it is connected to the interface helices at its ends and thus the conformational dynamics of the lid-loop are linked to GATase rotation. Following substrate binding, the lid-loop closes over the ATPPase active site thereby facilitating the formation of the adenyl-XMP intermediate through interactions involving His388 and His389. Apart from enabling the synthesis of adenyl-XMP intermediate, the closed conformation of the lid-loop forms a sealed pocket for ammonia tunnelling. This pocket creates a solvent-free environment protecting the adenyl-XMP intermediate from attack by water while also preventing the protonation of ammonia, which would render it incapable of carrying out the nucleophilic attack. The mutations of the XMP binding pocket not only shed light on the essentiality of dimerization in PfGMPS, but it also highlights the subtle differences in the substrate binding pocket of PfGMPS as compared to human GMPS

thus opening up avenues for designing drugs that are specific to the parasite enzyme. The findings emanating from these experiments constitute a significant addition to our understanding of this mechanistically intriguing and therapeutically relevant enzyme.

Materials and methods

Sequence and structure analysis

Protein sequences were retrieved from GenBank and UniProt sequence databases [42,43]. The sequence alignment was performed using the MAFFT web server [44], and the figure was generated using ESPript or the weblogo server [45,46]. The coordinates of the crystal structures of GMP synthetases were retrieved from RCSB Protein Data Bank [47]. The PDB IDs of the structures of GMPS analyzed are 1GPM (*Escherichia coli*), 3TQI (*Coxiella burnetii*), 2YWB and 2YWC (*Thermus thermophilus*), 5TW7 (*Neisseria gonorrhoeae*), 2VXO (*Homo sapiens*), 3UOW, 4WIM and 4WIO (*Plasmodium falciparum*). PyMOL was used to visualize and superpose structures, and generate figures [48]. H-bonds were identified using a distance cut-off of 3.2 Å between the donor and acceptor atoms. The negatively charged Asp, Glu residues were inferred to be forming a salt bridge with the positively charged Arg, Lys or His if the side chain carboxyl oxygen atoms of either Asp or Glu were within 4 Å of the side chain nitrogen atoms of Arg, His or Lys [49,50]. The atoms in the positively charged residues were Nζ in Lys; Nε, Nη1, or Nη2 in Arg, and Nδ1 or Nε2 in His. Every chain in a structure was analyzed independently. The disordered side chains were modelled using Swiss-PDB Viewer [51]. The modelled residues were then energy minimized using GROMOS96 force field implementation of Swiss-PDB Viewer, leaving the rest of the structure in the original conformation.

Site directed mutagenesis

Site-directed mutants of PfGMPS were generated using the pET_PfGMPS expression construct [29] as a template. The mutants were constructed using the protocol outlined in

Quikchange II site-directed mutagenesis kit (Agilent technologies) with minor modifications. The sequences of the primers used in the PCRs are in Table S3. Phusion DNA polymerase (Thermo Scientific) was used for the PCRs, and the products were treated with 20 units of DpnI (New England Biolabs) at 37 °C overnight to digest the methylated template DNA. *E. coli* XL1-Blue competent cells were transformed with the PCR products, and the presence of mutation as well as the absence of errors in the open reading frame was confirmed by sequencing.

Over-expression and purification of PfGMPS WT and mutants

The expression and purification of PfGMPS WT and mutants were performed as described earlier [30]. The WT was expressed using the pQE30_PfGMPS construct [28] in a GMPS knockout *E. coli* strain AT2465 (λ^-, *e14*−, *guaA21, relA1, spoT1* and *thiE1*) and the mutants were expressed in *E. coli* BL21-CodonPlus (DE3)-RIL cells transformed with pET_PfGMPS construct. The cells were grown in 4 l of terrific broth supplemented with 100 μg ml^{-1} ampicillin (WT) or 100 μg ml^{-1} ampicillin and 34 μg ml^{-1} chloramphenicol (mutants). Protein expression was induced by adding 0.5 mM isopropyl-β-D-thiogalactoside after the OD_{600} reached 0.8. The cells were harvested after 18 h of further incubation at 27 °C (WT) or 16 °C (mutants) by centrifugation. The cell pellet was resuspended in lysis buffer (50 mM Tris-HCl, pH 7.4, 10 % (v/v) glycerol, 2 mM β-mercaptoethanol) and stored at -80 °C.

The frozen cells were thawed on ice and supplemented with 2 mM β-mercaptoethanol and 1 mM phenylmethanesulfonyl fluoride. The cells were disrupted by sonication and the lysate was centrifuged at 30500 g, 4 °C for 45 min. The supernatant was loaded onto 2 ml HisTrap HP Ni-NTA column (GE Healthcare) connected to ÄKTA Basic HPLC (GE Healthcare). The column was pre-equilibrated with lysis buffer supplemented with 0.1 mM phenylmethanesulfonyl fluoride. The column with the bound protein was washed with step gradients of increasing imidazole concentration in lysis buffer and the bound proteins were

eluted by ramping the imidazole concentration to 500 mM. The eluted fractions were examined by 12 % (w/v) sodium dodecyl sulfate-polyacrylamide gel electrophoresis. The fractions containing PfGMPS in high amounts were pooled and concentrated using Amicon Ultra-15 centrifugal filters with 30 kDa cutoff membrane (Merck Millipore). The concentrated protein solution (about 2.5 ml) was injected into HiLoad 16/600 Superdex 200pg column (GE Healthcare) which was equilibrated with a buffer containing 20 mM Tris-HCl, pH 7.4, 10% (v/v) glycerol, 1 mM EDTA and 2 mM DTT. The flow rate employed was 0.3 ml min^{-1} and the eluted fractions were examined by 12 % (w/v) sodium dodecyl sulfate-polyacrylamide gel electrophoresis. The fractions containing pure protein were pooled, concentrated using centrifugal filters, flash-frozen in liquid nitrogen and stored in -80 °C freezer. The concentration of the protein was estimated using Bradford's assay [52].

Circular dichroism measurements

Far-UV circular dichroism spectra were recorded using a J-810 spectropolarimeter (Jasco) using a quartz cell with 1 mm path length. The spectra were recorded from 200 to 260 nm with a bandwidth of 1 nm and a scan speed of 20 nm min^{-1}. Each spectrum is an average of three scans. The concentration of the protein was 5 µM in a buffer containing 6.7 mM Tris-HCl, pH 7.4, 3.3 % (v/v) glycerol, 0.3 mM EDTA and 0.6 mM DTT.

Analytical size-exclusion chromatography

The oligomeric state of the protein was determined using analytical size-exclusion chromatography. An HR 10/30 column packed with Sephadex 300 matrix attached to an ÄKTA basic HPLC system equipped with a UV-900 detector was employed. The column was equilibrated with a buffer containing 50 mM Tris-HCl, pH 7.4, 100 mM KCl and calibrated with the protein standards β-amylase, alcohol dehydrogenase, bovine serum albumin, carbonic anhydrase and cytochrome c (Sigma-Aldrich). 100 µl of the protein sample

of concentration of 1 mg ml^{-1} was injected into the column individually and eluted at a flow rate of 0.5 ml min^{-1}. The eluted proteins were detected by monitoring absorbance at 220 nm.

Enzyme assays

Assay for measuring GMP formation

Gln and NH_4Cl dependent GMP synthesis were monitored at 25 °C using a continuous spectrophotometric assay as reported previously [28]. The reduction in absorbance due to the conversion of XMP to GMP was monitored at 290 nm using a Hitachi U2010 spectrophotometer. A Δε value of 1500 M^{-1} cm^{-1} was used to calculate the concentration of the product formed [53]. The standard assay consisted of 90 mM Tris-HCl, pH 8.5, 150 µM XMP, 2 mM ATP, 5 mM Gln, 20 mM $MgCl_2$, 0.1 mM EDTA and 0.1 mM DTT in a total reaction volume of 250 µl. To measure NH_4Cl dependent GMP formation, Gln in the reaction mix was replaced with 50 mM NH_4Cl. The reaction was initiated by adding PfGMPS WT or mutants to a final concentration of 0.92 µM in the reaction mix. The steady-state kinetic parameters were obtained by measuring initial velocities over a range of substrate concentrations. When the concentration of one substrate was varied, the concentration of the other two substrates was fixed at saturating levels. XMP concentration was uniformly fixed at 0.15 mM for WT and mutants. ATP concentration was fixed at 2 mM for WT and mutants except for PfGMPS_K415L where it was at 5 mM. Fixed Gln concentration varied across the enzymes with WT and K415L at 5 mM, 10 mM for R25L, 15 mM for D413A, 30 mM for E213A and K376L, 40 mM for K24L and 50 mM for D412A. This was done to ensure that the concentration of the fixed substrate was saturating for each of the mutants. Initial velocity data measured at various substrate concentrations were fitted to the Michaelis–Menten equation [$v=(v_{max}\times[S])/(K_{m(app)}+[S])$] by nonlinear regression using the software Prism 5 (GraphPad Software). A minimum of 10-14 substrate concentrations were used to determine

the kinetic parameters. The kinetic parameters were determined twice and the results were used to calculate the mean and SEM.

Assay for GATase activity

GATase activity was measured at 25 °C by estimating the concentration of glutamate formed using L-glutamate dehydrogenase (Sigma-Aldrich) as the coupling enzyme. In the coupled enzyme assay, the glutamate generated by the GATase domain is converted to α-ketoglutarate along with the concomitant reduction of NAD^+ to NADH. Hence, Glu formed was monitored as an increase in absorbance at 340 nm in a continuous spectrophotometric assay. The concentration of Glu produced was estimated using a Δε value of 6220 M^{-1} cm^{-1}. A 250 µl reaction mix contained 100 mM Tris-HCl, pH 8.5, 20 mM Gln, 150 µM XMP, 3 mM ATP, 20 mM $MgCl_2$, 0.5 mM NAD^+, 50 mM KCl, 0.1 mM EDTA and 0.1 mM DTT. The reaction mix was supplemented with an excess of L-glutamate dehydrogenase to ensure that the coupling enzyme was not limiting and the reaction was initiated by adding PfGMPS WT or mutants to a final concentration of 0.31 µM. The activity was expressed as a percentage of the activity of WT. The values from triplicate measurements were used to calculate the mean and SEM. This assay was also used to determine the binding affinities for ATP.Mg^{2+} and XMP in mutants that were inactive for GMP formation. However, mutants, which displayed < 40% GATase activation reported poorly in the coupled enzyme assay at low substrate concentrations and hence their binding affinities could not be measured.

Stopped-flow assay

Stopped-flow assay to detect the formation of the adenyl-XMP intermediate was performed as reported previously [30] using an SFM 300 stopped-flow device (BioLogic Science Instruments) equipped with MOS-200/M optics. The one-phase exponential decay in absorbance at 290 nm (A_{290}) corresponding to the formation of adenyl-XMP intermediate was monitored using a 150 W Xe(Hg) lamp as a light source and TC-100/10F cuvette which

provides a path length of 1 cm. The total flow rate was 8 ml s^{-1}, which resulted in a dead time of 3.8 ms. The instrument was controlled using Biokine32 software, version 4.62, which allows accumulation of 8000 data points for each trace. Data were acquired every ms, and traces from three or more shots were averaged. The A_{290} of the averaged data was normalized to set the initial offset to zero. The normalized A_{290} was plotted against time and the resulting plots were fitted to equation 1:

$$A_{290} = A_1 \times (e^{-k' t} - 1) - k'' t \qquad \text{(equation 1)}$$

where *k*' is the observed rate constant of the exponential phase corresponding to the formation of adenyl-XMP intermediate, *k*'' is the rate constant of the steady-state phase and A_1 is the amplitude of the exponential phase. A solution of 15 µM PfGMPS WT or mutants in 20 mM Tris-HCl, pH 7.4, 10 % (v/v) glycerol, 1 mM EDTA and 2 mM DTT was loaded in one syringe and the second syringe was loaded with a substrate mix containing 180 mM Tris-HCl, pH 8.5, 300 µM XMP, 4 mM ATP, 0.2 mM EDTA, 0.2 mM DTT and 40 mM $MgCl_2$. The two solutions were mixed in a 1:1 ratio at a total flow rate of 8 ml s^{-1} and the A_{290} changes were recorded as a function of time. For each mutant, the exponential phase rate constant *k*' was measured thrice and the *k*' expressed as mean and SEM.

References

[1] H. Zalkin, The Amidotransferases, Adv. Enzymol. Relat. Areas Mol. Biol. 66 (1993) 203–309.

[2] F. Massière, M.-A. Badet-Denisot, The mechanism of glutamine-dependent amidotransferases, Cell. Mol. Life Sci. 54 (1998) 205–222. doi:10.1007/s000180050145.

[3] F.M. Raushel, J.B. Thoden, H.M. Holden, The amidotransferase family of enzymes: Molecular machines for the production and delivery of ammonia, Biochemistry 38 (1999) 7891–7899. doi:10.1021/bi990871p.

[4] X. Huang, H.M. Holden, F.M. Raushel, Channeling of substrates and intermediates in enzyme-catalyzed reactions, Annu. Rev. Biochem. 70 (2001) 149–180. doi:10.1146/annurev.biochem.70.1.149.

[5] E.W. Miles, S. Rhee, D.R. Davies, The molecular basis of substrate channeling, J. Biol. Chem. 274 (1999) 12193–12196. doi:10.1074/jbc.274.18.12193.

[6] F.M. Raushel, J.B. Thoden, H.M. Holden, Enzymes with molecular tunnels, Acc. Chem. Res. 36 (2003) 539–548. doi:10.1021/ar020047k.

[7] S. Mouilleron, B. Golinelli-Pimpaneau, Conformational changes in ammonia-channeling glutamine amidotransferases, Curr. Opin. Struct. Biol. 17 (2007) 653–664. doi:10.1016/j.sbi.2007.09.003.

[8] J.L. Smith, Glutamine PRPP amidotransferase: Snapshots of an enzyme in action, Curr. Opin. Struct. Biol. 8 (1998) 686–694. doi:10.1016/S0959-440X(98)80087-0.

[9] C.L. Shelton, A.L. Lamb, Unraveling the Structure and Mechanism of the MST(ery) Enzymes, Trends Biochem. Sci. 43 (2018) 342–357. doi:10.1016/j.tibs.2018.02.011.

[10] N.G.J. Richards, M.S. Kilberg, Asparagine synthetase chemotherapy, Annu. Rev. Biochem. 75 (2006) 629–654. doi:10.1146/annurev.biochem.75.103004.142520.

[11] T.A. Walsh, T. Bauer, R. Neal, A.O. Merlo, P.R. Schmitzer, G.R. Hicks, M. Honma, W. Matsumura, K. Wolff, J.P. Davies, Chemical genetic identification of glutamine phosphoribosylpyrophosphate amidotransferase as the target for a novel bleaching herbicide in Arabidopsis, Plant Physiol. 144 (2007) 1292–1304. doi:10.1104/pp.107.099705.

[12] B.M. Mailu, L. Li, J. Arthur, T.M. Nelson, G. Ramasamy, K. Fritz-Wolf, K. Becker, M.J. Gardner, *Plasmodium* apicoplast Gln-tRNA^{Gln} biosynthesis utilizes a unique GatAB amidotransferase essential for erythrocytic stage parasites, J. Biol. Chem. 290 (2015) 29629–29641. doi:10.1074/jbc.M115.655100.

[13] Q. Li, C. Leija, F. Rijo-Ferreira, J. Chen, I. Cestari, K. Stuart, B.P. Tu, M.A. Phillips, GMP synthase is essential for viability and infectivity of *Trypanosoma brucei* despite a redundant purine salvage pathway, Mol. Microbiol. 97 (2015) 1006–1020. doi:10.1111/mmi.13083.

[14] H. Zalkin, J.L. Smith, Enzymes utilizing glutamine as an amide donor, Adv. Enzymol. Relat. Areas Mol. Biol. 72 (1998) 87–144.

[15] L. David, E. Cheah, M. Cygler, B. Dijkstra, F. Frolow, M. Sybille, M. Harel, S. James Remington, I. Silman, J. Schrag, H.G.V. Koen, A. Goldman, The α/β hydrolase fold, Protein Eng. Des. Sel. 5 (1992) 197–211. doi:10.1093/protein/5.3.197.

[16] B.N. Chaudhuri, S.C. Lange, R.S. Myers, V.J. Davisson, J.L. Smith, Toward understanding the mechanism of the complex cyclization reaction catalyzed by imidazole glycerolphosphate synthase: Crystal structures of a ternary complex and the free enzyme, Biochemistry 42 (2003) 7003–7012. doi:10.1021/bi034320h.

[17] J.B. Thoden, H.M. Holden, G. Wesenberg, F.M. Raushel, I. Rayment, Structure of carbamoyl phosphate synthetase: A journey of 96 Å from substrate to product, Biochemistry 36 (1997) 6305–6316. doi:10.1021/bi970503q.

[18] R. Anand, A.A. Hoskins, J. Stubbe, S.E. Ealick, Domain organization of *Salmonella typhimurium* formylglycinamide ribonucleotide amidotransferase revealed by X-ray crystallography, Biochemistry. 43 (2004) 10328–10342. doi:10.1021/bi0491301.

[19] J.A. Endrizzi, H. Kim, P.M. Anderson, E.P. Baldwin, Crystal structure of *Escherichia coli* cytidine triphosphate synthetase, a nucleotide-regulated glutamine amidotransferase/ATP-dependent amidoligase fusion protein and homologue of anticancer and antiparasitic drug targets, Biochemistry 43 (2004) 6447–6463. doi:10.1021/bi0496945.

[20] Q.-A. Li, D.V. Mavrodi, L.S. Thomashow, M. Roessle, W. Blankenfeldt, Ligand binding induces an ammonia channel in 2-amino-2-desoxyisochorismate (ADIC) synthase PhzE, J. Biol. Chem. 286 (2011) 18213–18221. doi:10.1074/jbc.M110.183418.

[21] T. Knöchel, A. Ivens, G. Hester, A. Gonzalez, R. Bauerle, M. Wilmanns, K. Kirschner, J.N. Jansonius, The crystal structure of anthranilate synthase from *Sulfolobus solfataricus*: Functional implications, Proc. Natl. Acad. Sci. U.S.A. 96 (1999) 9479–9484. doi:10.1073/pnas.96.17.9479.

[22] J.J.G. Tesmer, T.J. Klem, M.L. Deras, V.J. Davisson, J.L. Smith, The crystal structure of GMP synthetase reveals a novel catalytic triad and is a structural paradigm for two enzyme families, Nat. Struct. Biol. 3 (1996) 74–86. doi:10.1038/nsb0196-74.

[23] F. Zein, Y. Zhang, Y.-N. Kang, K. Burns, T.P. Begley, S.E. Ealick, Structural insights into the mechanism of the PLP synthase holoenzyme from *Thermotoga maritima*, Biochemistry 45 (2006) 14609–14620. doi:10.1021/bi061464y.

[24] M. Strohmeier, T. Raschle, J. Mazurkiewicz, K. Rippe, I. Sinning, T.B. Fitzpatrick, I. Tews, Structure of a bacterial pyridoxal 5′-phosphate synthase complex, Proc. Natl. Acad. Sci. U.S.A. 103 (2006) 19284–19289. doi:10.1073/pnas.0604950103.

[25] A.S. Tanwar, D.J. Sindhikara, F. Hirata, R. Anand, Determination of the formylglycinamide ribonucleotide amidotransferase ammonia pathway by combining 3d-rism theory with experiment, ACS Chem. Biol. 10 (2015) 698–704. doi:10.1021/cb501015r.

[26] E.M. Lynch, D.R. Hicks, M. Shepherd, J.A. Endrizzi, A. Maker, J.M. Hansen, R.M. Barry, Z. Gitai, E.P. Baldwin, J.M. Kollman, Human CTP synthase filament structure reveals the active enzyme conformation, Nat. Struct. Mol. Biol. 24 (2017) 507–514. doi:10.1038/nsmb.3407.

[27] M. Welin, L. Lehtiö, A. Johansson, S. Flodin, T. Nyman, L. Trésaugues, M. Hammarström, S. Gräslund, P. Nordlund, Substrate specificity and oligomerization of human GMP synthetase, J. Mol. Biol. 425 (2013) 4323–4333. doi:10.1016/j.jmb.2013.06.032.

[28] J.Y. Bhat, B.G. Shastri, H. Balaram, Kinetic and biochemical characterization of *Plasmodium falciparum* GMP synthetase, Biochem. J. 409 (2008) 263–273. doi:10.1042/BJ20070996.

[29] J.Y. Bhat, R. Venkatachala, K. Singh, K. Gupta, S.P. Sarma, H. Balaram, Ammonia channeling in *Plasmodium falciparum* GMP synthetase: investigation by NMR spectroscopy and biochemical assays, Biochemistry 50 (2011) 3346–3356. doi:10.1021/bi1017057.

[30] L. Ballut, S. Violot, S. Shivakumaraswamy, L.P. Thota, M. Sathya, J. Kunala, B.W. Dijkstra, R. Terreux, R. Haser, H. Balaram, H. Balaram, N. Aghajari, Active site coupling in *Plasmodium falciparum* GMP synthetase is triggered by domain rotation, Nat. Commun. 6 (2015). doi:10.1038/ncomms9930.

[31] R. Ali, S. Kumar, H. Balaram, S.P. Sarma, Solution nuclear magnetic resonance structure of the GATase subunit and structural basis of the interaction between

GATase and ATPPase subunits in a two-subunit-type GMPS from *Methanocaldococcus jannaschii*, Biochemistry 52 (2013) 4308–4323. doi:10.1021/bi400472e.

[32] J.C. Oliver, R. Gudihal, J.W. Burgner, A.M. Pedley, A.T. Zwierko, V.J. Davisson, R.S. Linger, Conformational changes involving ammonia tunnel formation and allosteric control in GMP synthetase, Arch. Biochem. Biophys. 545 (2014) 22–32. doi:10.1016/j.abb.2014.01.004.

[33] K.N. Allen, D. Dunaway-Mariano, Catalytic scaffolds for phosphoryl group transfer, Curr. Opin. Struct. Biol. 41 (2016) 172–179. doi:10.1016/j.sbi.2016.07.017.

[34] J.K. Lassila, J.G. Zalatan, D. Herschlag, Biological phosphoryl-transfer reactions: Understanding mechanism and catalysis, Annu. Rev. Biochem. 80 (2011) 669–702. doi:10.1146/annurev-biochem-060409-092741.

[35] S. Schmelz, J.H. Naismith, Adenylate-forming enzymes, Curr. Opin. Struct. Biol. 19 (2009) 666–671. doi:10.1016/j.sbi.2009.09.004.

[36] A. Yaremchuk, I. Kriklivyi, M. Tukalo, S. Cusack, Class I tyrosyl-tRNA synthetase has a class II mode of cognate tRNA recognition, EMBO J. 21 (2002) 3829–3840. doi:10.1093/emboj/cdf373.

[37] T. Kobayashi, T. Takimura, R. Sekine, K. Vincent, K. Kamata, K. Sakamoto, S. Nishimura, S. Yokoyama, Structural snapshots of the KMSKS loop rearrangement for amino acid activation by bacterial tyrosyl-tRNA synthetase, J. Mol. Biol. 346 (2005) 105–117. doi:10.1016/j.jmb.2004.11.034.

[38] J. Nakamura, L. Lou, Biochemical characterization of human GMP synthetase, J. Biol. Chem. 270 (1995) 7347–7353. doi:10.1074/jbc.270.13.7347.

[39] J.L. Chitty, T.L. Tatzenko, S.J. Williams, Y.Q.A.E. Koh, E.C. Corfield, M.S. Butler, A.A.B. Robertson, M.A. Cooper, U. Kappler, B. Kobe, B. Kobe, J.A. Fraser, GMP synthase is required for virulence factor production and infection by *Cryptococcus neoformans*, J. Biol. Chem. 292 (2017) 3049–3059. doi:10.1074/jbc.M116.767533.

[40] T.M.A. Franco, D.C. Rostirolla, R.G. Ducati, D.M. Lorenzini, L.A. Basso, D.S. Santos, Biochemical characterization of recombinant guaA-encoded guanosine monophosphate synthetase (EC 6.3.5.2) from *Mycobacterium tuberculosis* H37Rv strain, Arch. Biochem. Biophys. 517 (2012) 1–11. doi:10.1016/j.abb.2011.11.013.

[41] N. Sakamoto, G.W. Hatfield, H.S. Moyed, Physical properties and subunit structure of xanthosine 5'-phosphate aminase, J. Biol. Chem. 247 (1972) 5880–5887.

[42] D.A. Benson, I. Karsch-Mizrachi, K. Clark, D.J. Lipman, J. Ostell, E.W. Sayers, GenBank, Nucleic Acids Res. 40 (2012) D48-53. doi:10.1093/nar/gkr1202.

[43] Uniprot Consortium, UniProt: A worldwide hub of protein knowledge, Nucleic Acids Res. 47 (2019) D506–D515. doi:10.1093/nar/gky1049.

[44] K. Katoh, J. Rozewicki, K.D. Yamada, MAFFT online service: multiple sequence alignment, interactive sequence choice and visualization, Brief. Bioinformatics 20 (2019) 1160–1166. doi: 10.1093/bib/bbx108.

[45] P. Gouet, E. Courcelle, D.I. Stuart, F. Métoz, ESPript: Analysis of multiple sequence alignments in PostScript, Bioinformatics 15 (1999) 305–308. doi:10.1093/bioinformatics/15.4.305.

[46] G.E. Crooks, G. Hon, J.-M. Chandonia, S.E. Brenner, WebLogo: A sequence logo generator, Genome Res. 14 (2004) 1188–1190. doi:10.1101/gr.849004.

[47] H.M. Berman, J. Westbrook, Z. Feng, G. Gilliland, T.N. Bhat, H. Weissig, I.N. Shindyalov, P.E. Bourne, The Protein Data Bank, Nucleic Acids Res. 28 (2000) 235–242. doi:10.1093/nar/28.1.235

[48] L.L.C. Schrödinger, The PyMOL Molecular Graphics System, (2010).

[49] D.J. Barlow, J.M. Thornton, Ion-pairs in proteins, J. Mol. Biol. 168 (1983) 867–885. doi:10.1016/S0022-2836(83)80079-5.

[50] J.N. Sarakatsannis, Y. Duan, Statistical characterization of salt bridges in proteins, Proteins Struct. Funct. Genet. 60 (2005) 732–739. doi:10.1002/prot.20549.

[51] N. Guex, M.C. Peitsch, SWISS-MODEL and the Swiss-PdbViewer: An environment for comparative protein modeling, Electrophoresis 18 (1997) 2714–2723. doi:10.1002/elps.1150181505.

[52] M.M. Bradford, A rapid and sensitive method for the quantitation of microgram quantities of protein utilizing the principle of protein-dye binding, Anal. Biochem. 72 (1976) 248–254. doi:10.1016/0003-2697(76)90527-3.

[53] H.S. Moyed, B. Magasanik, Enzymes essential for the biosynthesis of nucleic acid guanine; xanthosine 5'-phosphate aminase of *Aerobacter aerogenes*, J. Biol. Chem. 226 (1957) 351–363.

Declarations of interest

The authors declare no competing financial interests.

Author Contributions

SS- conceptualization, structure and sequence analysis, construction of mutants and protein purification, enzyme kinetics, data analysis; NP- construction of mutants and protein purification, enzyme kinetics; LB, SV and NA- solved the structures of PfGMPS used in this study; HB- conceptualization, structure and sequence analyses, data analysis. SS and HB wrote the manuscript with critical inputs from NA.

Acknowledgements

We acknowledge the constructive criticism offered by Lakshmeesha K. N.

Footnotes

This project was funded by the Department of Biotechnology, Ministry of Science and Technology, Government of India Grants BT/PR11294/BRB/10/1291/2014, BT/PR13760/COE/34/42/2015, and BT/INF/22/SP27679/ 2018; Science and Engineering Research Board, Department of Science and Technology, Government of India Grant EMR/2014/001276; and institutional funding from the Jawaharlal Nehru Centre of Advanced Scientific Research, Department of Science and Technology, India. SS was supported by University Grants Commission junior and senior research fellowships. NP is supported by Indian Council of Medical Research junior research fellowship. HB is a recipient of JC Bose National Fellowship from the Government of India. NA acknowledges funding from the CNRS, the ANR project grant "PLASMOPUR" ANR-17-CE11-0032 and the Fondation Innovation en Infectiologie, "FINOVI project AO12-27").

Figure Legends

Figure 1. Conformational dynamics of GATase domain in PfGMPS. (a) Crystal structure of XMP complexed PfGMPS (PDB ID 3UOW) with the GATase domain in 0° rotated state. (b) Crystal structure of Gln complexed PfGMPS (PDB ID 4WIO) with the GATase domain in 85° rotated state. The 0° structure shown in (a) is superposed on this structure to highlight rotation of the GATase domain. The backbone is shown in ribbon representation with the GATase and ATPPase domains coloured green and purple, respectively. The ligands XMP (cyan), Gln (orange), AMP (magenta) and PPi (yellow) are shown as spheres. Gln in (a) is superposed from 4WIO and XMP in panel (b) is from 3UOW. AMP and PPi in both panels are superposed from the crystal structure of EcGMPS (PDB ID 1GPM). In both (a) and (b), residues on GATase and ATPPase domains that are with 4 Å distance cutoff from each other are shown as lines.

Figure 2. Reaction catalyzed by GMPS (a), ATPPase domain (b) and GATase domain (c).

Figure 3. Interdomain interactions in PfGMPS. (a) Schematic showing the relative location of the various conserved motifs that are examined in this study. The interface helices are shown as squiggles. The sequence of conserved motifs in PfGMPS, as well as the frequency of occurrence of a residue in the multiple sequence alignment (Fig. S2) are shown. The residues investigated by site-directed mutagenesis in this and an earlier study [30] are shown as stars and circles, respectively. The location of the GATase catalytic triad residues is also shown. (b) Helices α1, α11 and α12 in the interdomain interface in the 0° structure of PfGMPS (PDB ID 3UOW). (c) Interdomain salt bridges in the 0° structures. The chain A in structure 3UOW is superposed on chain B of 4WIM (apo PfGMPS), which is shown in a lighter shade of colour. (d) Helices α11 and α12 in the interdomain interface in 85° GATase rotated PfGMPS structure (PDB ID 4WIO). (e) Interdomain salt bridges in the 85° rotated structure. In all the images, the GATase and ATPPase domains are coloured green and

purple, respectively. The backbone is shown as line in (b, d, e) and as ribbon in (c). The disordered lid-loop is shown as a dashed line.

Figure 4. GATase activation and adenyl-XMP formation in PfGMPS WT and mutants. (a) Magnitude of GATase activation estimated using a coupled enzyme assay. GATase activity was measured using 20 mM Gln, 3 mM ATP.Mg^{2+} and 150 μM XMP. The specific activity values are normalized to the GATase activity of the WT. The error bars represent the SEM of data from three measurements. (b) Rate (*k*') of adenyl-XMP formation measured using a stopped-flow spectrophotometer. The error bars represent the SEM of data from three independent measurements of *k*'. The concentration of the enzyme used was 7.5 μM and the concentration of ATP.Mg^{2+} and XMP were 2 mM and 0.15 mM, respectively. PfGMPS mutant is indicated by the residue, location in sequence and the residue to which it is mutated.

Figure 5. Interactions of residues on interface helices α1, α11 and α12 that point away from domain interface. (a) Interactions of Arg25 on α1 in XMP complexed PfGMPS structure (PDB ID 3UOW). The protein backbone is shown as ribbon with α1 coloured green and the loop containing catalytic His208 and Glu210 in pink. The substrate Gln (superposed from 4WIO) is shown in ball and stick representation. Residues on α1 and the loop that are located within 4 Å of each other are shown as lines. (b) Interactions of Lys411 on α12 in apo PfGMPS structure (PDB ID 4WIM). AMP, PPi (ball and stick) and Mg^{2+} (sphere) are superposed from the crystal structure of EcGMPS (PDB ID 1GPM). The helices α11 and α12 are coloured red and purple, respectively.

Figure 6. Role of lid-loop residues in adenyl-XMP formation. (a) Superposition of the ATPPase domain of XMP bound PfGMPS (magenta, PDB ID 3UOW) on the ATPPase domain of PfGMPS_C89A/Gln (green, PDB ID 4WIO). The lid-loop in PfGMPS_C89A/Gln is highlighted for reference. (b) Interactions of residues on the lid-loop with AMP in the structure of PfGMPS_C89A/Gln. In both (a) and (b), AMP and PPi are superposed from

EcGMPS (PDB ID 1GPM). Protein backbone is in ribbon and ligands are in ball and stick representation. (c) Stopped-flow progress curves for the formation of adenyl-XMP intermediate. Shown are absorbance values at 290 nm as a function of time (points) and fit of the data (solid lines) to one-phase exponential decay equation. The concentrations used were 7.5 μM enzyme, 2 mM ATP.Mg^{2+} and 0.15 mM XMP.

Figure 7. Interactions of the C-terminal loop in PfGMPS (PDB ID 3UOW). (a) Interactions with XMP. (b) Interdimer interactions of Arg539 from a neighbouring chain with residues on C-terminal loop. In both images, the protein backbone is in ribbon representation with chain A coloured green and chain B orange. The C-terminal loop of chain A is coloured magenta. XMP is shown as ball and stick and highlighted residues are shown as sticks.

Figure 8. Connectivity through the protein couples catalysis with allostery. (a) Overview of key residues involved in substrate binding, interdomain and intersubunit crosstalk in PfGMPS. Structure of XMP bound PfGMPS (PDB ID 3UOW) with critical residues in stick representation. The GATase domain is shown in green except for the catalytic Cys and loop containing His and Glu of the catalytic triad that is in blue. The ATPPase core and dimerization domains are in orange and pink, respectively. The Arg539 from the neighbouring monomer is shown in cyan. The helix α11, the lid-loop and helix α12 are in grey. The ligands XMP and AMP+PPi (superposed from 1GPM) are shown in ball and stick representation. The position of residues Lys386, His388 and His389 are from superposition of the crystal structure of PfGMPS_C89A/Gln (PDB ID 4WIO) onto that of the XMP bound PfGMPS. Dashed lines represent H-bonds with distances indicated in Å. Red and blue arrows point to residues involved in adenyl-XMP formation and GATase-ATPPase interactions, respectively. (b) Simplified schematic illustrating the coupling of catalysis in ATPPase domain with allostery. Residues on ATPPase helices α11 and α12 that face the ATPPase pocket along with those on the lid-loop play roles in binding of substrates and formation of

the adenyl-XMP intermediate. The residues on α11 and α12 that face the interface form salt bridges with residues on GATase helix α1. Key inter-residue and protein-ligand interactions are shown as brown and blue dashes, respectively.

Figure S1. Overview of experiments performed using PfGMPS WT and mutants. PfGMPS mutant is indicated by the residue, its location in sequence and the residue to which it is mutated. (a) SDS-PAGE of purified proteins. 30 µg of the protein was loaded in all cases except PfGMPS_D413A where 15 µg was loaded. The mutant Y212A is not part of this study. Lane M, molecular mass standards with mass indicated in kDa. (b) The far-UV CD spectra recorded using 5 µM of protein in a buffer containing 6.7 mM Tris-HCl, pH 7.4, 3.3 % (v/v) glycerol, 0.3 mM EDTA and 0.6 mM DTT. (c) Analytical size-exclusion chromatography to determine the oligomeric state. 100 µl of protein (1 mg ml^{-1}) was injected into a column (10 x 300 mm) packed with Sephadex300. The mutants K411L and D413A of PfGMPS were not examined by analytical size-exclusion chromatography. (d) Scheme illustrating the enzymatic assays performed using the WT and mutant PfGMPS.

Figure S2. Multiple sequence alignment of GMP synthetases from different organisms. Only the conserved blocks corresponding to the helices α1, α11, α12, lid-loop, C-terminal loop and residues Glu213 and Arg539 extracted from the full alignment are shown. Numbering corresponds to PfGMPS sequence. Invariant residues are highlighted by red/ white inversion and positions with high sequence similarity are shown in red and boxed in blue.

Table 1. Steady-state kinetic parameters of PfGMPS WT and mutants.

Varied substrate		WT	K24L	R25L	K160L	E213A	K376L	K411L	D412A	D413A	K415L
Gln	$K_{m(app)}$ (mM)	0.33 ± 0.02	1.75 ± 0.06 5.3 × ↑	0.47 ± 0.01	0.36 ± 0.004	1.29 ± 0.04 3.9 × ↑	1.46 ± 0.07 4.4 × ↑	Inactive	2.61 ± 0.22 7.9 × ↑	1.19 ± 0.1 3.6 × ↑	0.25 ± 0.01
	k_{cat} (min^{-1})	45.9 ± 0.3	17.8 ± 0.4 2.6 × ↓	46.6 ± 1.8	49.9 ± 0.4	47.6 ± 1.6	48.3 ± 1.3		39.4 ± 0.3	35.1 ± 0.5	42.4 ± 0.2
ATP	$K_{m(app)}$ (μM)	119 ± 2	67 ± 3 1.8 × ↓	117 ± 4	148 ± 3	162 ± 2	122 ± 0.1		96 ± 5	102 ± 1	500 ± 11 4.2 × ↑
	k_{cat} (min^{-1})	53.6 ± 2.4	20.4 ± 0.2 2.6 × ↓	49.9 ± 0.2	49.2 ± 1.2	50.8 ± 0.6	52.3 ± 0.5		43.4 ± 1.3	35.9 ± 1.7 1.5 × ↓	44 ± 1.1
XMP	$K_{m(app)}$ (μM)	7.1 ± 1	20.6 ± 1 2.9 × ↑	6.3 ± 0.4	12.7 ± 0.6 1.8 × ↑	13.1 ± 1 1.8 × ↑	12.1 ± 0.6 1.7 × ↑		9.5 ± 1.9	20 ± 2.9 2.8 × ↑	14.4 ± 1.5 2 × ↑
	k_{cat} (min^{-1})	44.4 ± 3.5	19.6 ± 0.3 2.3 × ↓	45.1 ± 4.2	56.2 ± 2.1	53.5 ± 1.5	57.4 ± 1.7		38 ± 3.5	31.9 ± 0.6	44.6 ± 3.5
NH_4Cl	$K_{m(app)}$ (mM)	25.6 ± 2.8	20.3 ± 2.1	13.1 ± 1.1 2 × ↓	23.6 ± 0.6	12.3 ± 0.4 2.1 × ↓	36.2 ± 2.2		38.9 ± 0.2 1.5 × ↑	12.2 ± 1.4 2.1 × ↓	17 ± 0.3 1.5 × ↓
	k_{cat} (min^{-1})	64.8 ± 6.4	27.9 ± 0.7 2.3 × ↓	56.3 ± 0.2	74.4 ± 1.6	42.5 ± 0.1 1.5 × ↓	47.5 ± 4.4		63.2 ± 1.8	42.6 ± 1.5 1.5 × ↓	35.5 ± 0.5 1.8 × ↓

The values are expressed as mean ± SEM of two independent experiments. The fold increase or decrease compared to the value for the WT is indicated by a number followed by an upward or downward arrow, respectively. Only changes ≥ 1.5-fold are indicated. The assay involved monitoring the decrease in absorbance at 290 nm arising from the conversion of XMP to GMP at 25 °C.

Table 2. Gln and NH_4Cl dependent GMP formation by PfGMPS lid-loop mutants.

Enzyme	**Specific activity (nmol min^{-1} mg^{-1})**	
	Gln dependent GMP formation	NH_4Cl dependent GMP formation
WT	658 ± 19	700 ± 22
K386L	8.1 ± 0.2	11 ± 0.1
T387A	526 ± 14	525 ± 0.5
H388A	0.9	3.4
H389A	3 ± 0.2	4 ± 0.1
N390A	No Activity	No Activity

The substrate concentrations used were 2 mM ATP.Mg^{2+}, 150 μM XMP and 0.5 mM Gln or 50 mM NH_4Cl.

Table S1. List of interdomain electrostatic interactions in the crystal structures of GMP synthetases where the GATase domain is not rotated (0° rotated structure).

	Chains	24 (K/R)(K/R)XRE 28	371 DXXES 375	411 KD(D/E)V(K/R) 415
E. coli (PDB ID: 1GPM)	A, B, C, D	25 RRVRE 29	340 DVIES 344	381 KDEVRK 386
		Arg25		Asp382 [A 2.8, B 3.1, C 2.9, D 5.1]
		Arg28		Glu383 [A 2.8, B 2.6, C 2.8, D 2.6]
		Glu29		Lys386 [A 5.8, B 5.5, C 5.1, D 5.6]
C. burnetii (PDB ID: 3TQI)	A, B, C, D	25 RRVRE 29	339 DVIES 343	380 KDEVRK 385
		Arg25		Asp381 [A 3.1, B 3.3, C 3.6, D 2.8]
		Arg28		Glu382 [A 3.0, B 2.8, C 2.7, D 2.9]
		Glu29		Lys385 [A 5.6, B 4.4, C 5.8, D 5.7]
T. thermophilus (PDB ID: 2YWB)	A	13 RLIARRLRELR 23	320 DVIES 324	359 KDEVRE 364
	B, D	13 RLIARRLRELR 23	320 DVIES 324	359 KDEVRE 364
	C	13 RLIARRLRELR 23	320 DVIES 324	359 KDEVRE 364
		Arg17		Asp360 [A 2.6, B 3.6, C 3.3, D 3.2]
		Arg20		Glu361 [B 2.9, C 2.9, D 2.9]
T. thermophilus (PDB ID: 2YWC)	A	13 RLIARRLRELR 23	320 DVIES 324	359 KDEVRE 364
	B, C, D	13 RLIARRLRELR 23	320 DVIES 324	359 KDEVRE 364
		Arg17		Asp360 [A 3.2, B 3.8, C 4.1, D 3.9]
		Arg20		Glu361 [A 2.7, B 2.9, C 2.9, D 2.9]
N. gonorrhoeae (PDB ID: 5TW7)	A, B, C, D	17 RLIARRVREAH 27	330 DVIES 334	371 KDEVRE 376
		Arg21		Asp372 [A 5.2, B 4.9, C 5.5, D 5.0]
		Arg24		Glu373 [A 2.7, B 2.7, C 2.9, D 2.8]
		His27		Glu376 [A 5.4, B 6.0, C 5.5]
		Arg17	Glu333 [C 3.1]	
H. sapiens (PDB ID: 2VXO)	A, B	39 KVIDRRVRE 47	372 DLIES 376	415 HKDEVR 420
		Asp42		His415 [A 5.5, B 5.5]
		Arg43		Asp417 [B 3.0]
		Arg46		Asp417 [A 5.3, B 5.0]
		Arg46		Glu418 [A 3.1, B 3.1]
P. falciparum (PDB ID: 3UOW)	A	20 HLIVKRLNNIK 30	371 DIIESK 376	411 KDDVK 415
		Lys24		Asp413 (5.0)
		Lys24		Asp412 (2.7)
	B	20 HLIVKRLNNIK 30	371 DIIESK 376	411 KDDVK 415
		His20	Glu374 (2.9)	
		Lys24		Asp413 (4.3)
		Lys24		Asp412 (5.9)
P. falciparum	A	20 HLIVKRLNNIK 30	371 DIIESK 376	411 KDDVK 415

(PDB ID: 4WIM)		His20	Glu374 (4.2)	
		Lys24		Asp413 (2.8)
	B	20 HLIVKRLNNIK 30	371 DIIESK 376	411 KDDVK 415
		Lys24		Asp412 (5.3)

The signature sequence with the numbering corresponding to PfGMPS is mentioned at the top of the table (green). The amino acid sequence of the helices α1, α11 and α12 for every chain analyzed (orange) is mentioned, and the residues corresponding to the signature sequence are underlined. In cases where the side chain of a residue or the entire residue is disordered, the residue is coloured purple. The distance between the salt bridge forming residues in different chains is specified in square brackets. Distances greater than 4.0 Å are highlighted in red.

Table S2. K_d values for ATP.Mg^{2+} and XMP for the lid-loop mutants

	***K*$_d$ (μM)**	
	ATP.Mg^{2+}	**XMP**
WT (*K*$_{m(app)}$)	119 ± 2	7.1 ± 1
H388A	9.2 ± 1.8	0.16 ± 0.03
H389A	75.6 ± 31.8	0.77 ± 0.004
N390A	2.2 ± 0.2	0.04 ± 0.0004

The K_d was determined by measuring GATase activity at various concentrations of either ATP.Mg^{2+} or XMP while maintaining the other substrate at fixed saturating concentration which was either 3 mM of ATP.Mg^{2+} or 150 μM of XMP. The glutamate produced was estimated using glutamate dehydrogenase as the coupling enzyme. The mean ± SEM of two experiments is reported.

Table S3: Sequences of primers used for site-directed mutagenesis.

Mutation	Primer sequence (5'-3')
K24L	CTTCCATTTGATTGTATTAAGATTAAACAATATAAAAATATTTAG
	CTAAATATTTTTATATTGTTTAATCTTAATACAATCAAATGGAAG
R25L	CTTCCATTTGATTGTAAAATTATTAAACAATATAAAAATATTTAGTG
	CACTAAATATTTTTATATTGTTTAATAATTTTACAATCAAATGGAAG
K160L	GTTTATTTGAAAATATTTTAAGTGACATTACAACGGTTTG
	CAAACCGTTGTAATGTCACTTAAAATATTTTCAAATAAAC
E213A	CATCCAGAGGTGTATGCATCATTAGATGGAGAATTAATG
	CATTAATTCTCCATCTAATGATGCATACACCTCTGGATG
K376L	CCAGATATTATTGAAAGTTTATGTTCAAAAAATTTATCAG
	CTGATAAATTTTTTGAACATAAACTTTCAATAATATCTGG
K386L	CAAAAAATTTATCAGATACTATTTTAACTCATCATAATGTAGG
	CCTACATTATGATGAGTTAAAATAGTATCTGATAAATTTTTTG
T387A	CAAAAAATTTATCAGATACTATTAAAGCTCATCATAATGTAGGAG
	CTCCTACATTATGATGAGCTTTAATAGTATCTGATAAATTTTTTG
H388A	CAGATACTATTAAAACTGCTCATAATGTAGGAGGCTTACC
	GGTAAGCCTCCTACATTATGAGCAGTTTTAATAGTATCTG
H389A	CAGATACTATTAAAACTCATGCTAATGTAGGAGGCTTACC
	GGTAAGCCTCCTACATTAGCATGAGTTTTAATAGTATCTG
N390A	CAGATACTATTAAAACTCATCATGCTGTAGGAGGCTTACC
	GGTAAGCCTCCTACAGCATGATGAGTTTTAATAGTATCTG
K411L	GAACCTTTCAAATATTTATTTTTAGATGATGTTAAAACATTATC
	GATAATGTTTTAACATCATCTAAAAATAAATATTTGAAAGGTTC
D412A	CCTTTCAAATATTTATTTAAAGCTGATGTTAAAACATTATC
	GATAATGTTTTAACATCAGCTTTAAATAAATATTTGAAAGG
D413A	CCTTTCAAATATTTATTTAAAGATGCTGTTAAAACATTATCTAGAG
	CTCTAGATAATGTTTTAACAGCATCTTTAAATAAATATTTGAAAGG
K415L	CCTTTCAAATATTTATTTAAAGATGATGTTTTAACATTATCTAGAG
	CTCTAGATAATGTTAAAACATCATCTTTAAATAAATATTTGAAAGG
R539L	GTGAAGTAAAGGGCGTCAACTTAATATTATATGATGTATCATC
	GATGATACATCATATAATATTAAGTTGACGCCCTTTACTTCAC
K547L	GAATATTATATGATGTATCATCATTACCACCAGCAACGATTG
	CAATCGTTGCTGGTGGTAATGATGATACATCATATAATATTC
E553L	CAAAACCACCAGCAACGATTTTATTCGAATGAGAGCTC
	GAGCTCTCATTCGAATAAAATCGTTGCTGGTGGTTTTG
E555L	GCAACGATTGAATTCTTATGAGAGCTCCGTCG
	CGACGGAGCTCTCATAAGAATTCAATCGTTGC

(a)

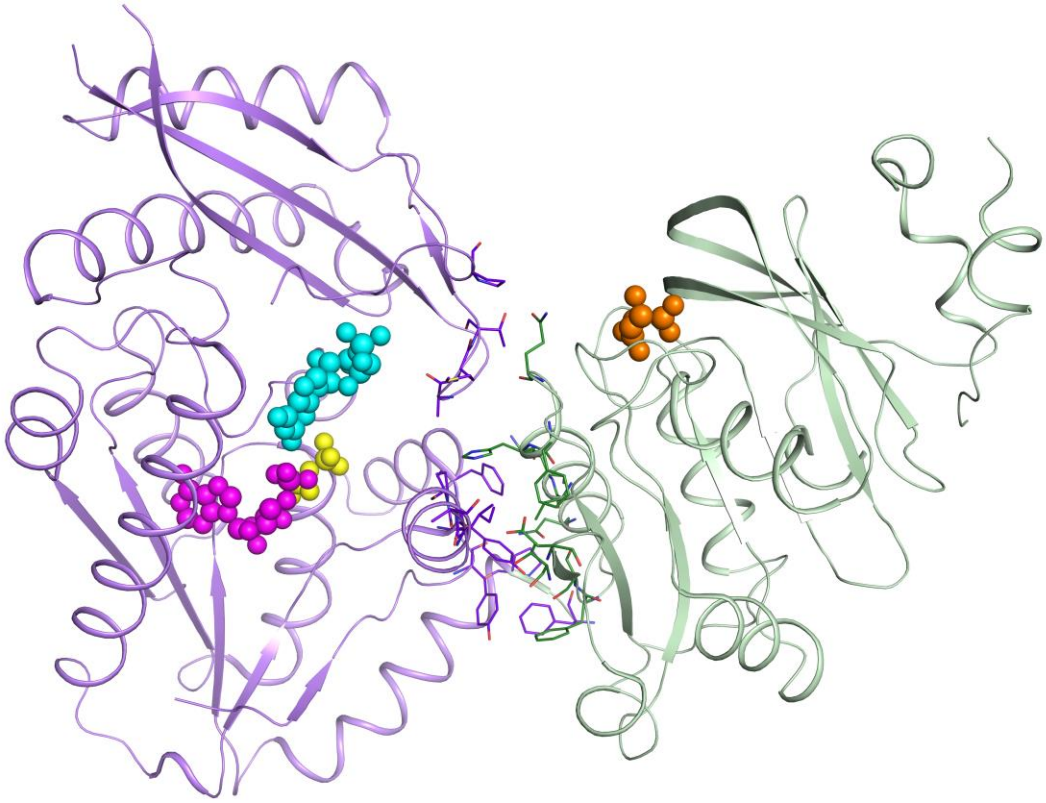

(b)

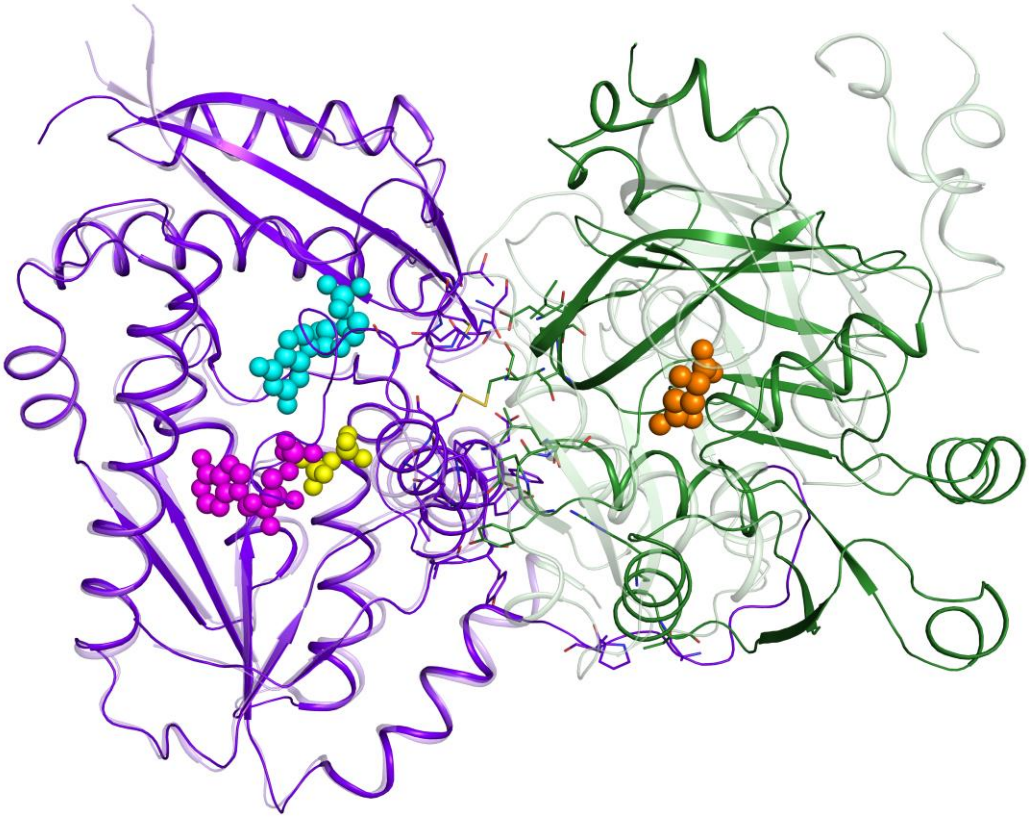

Figure 1

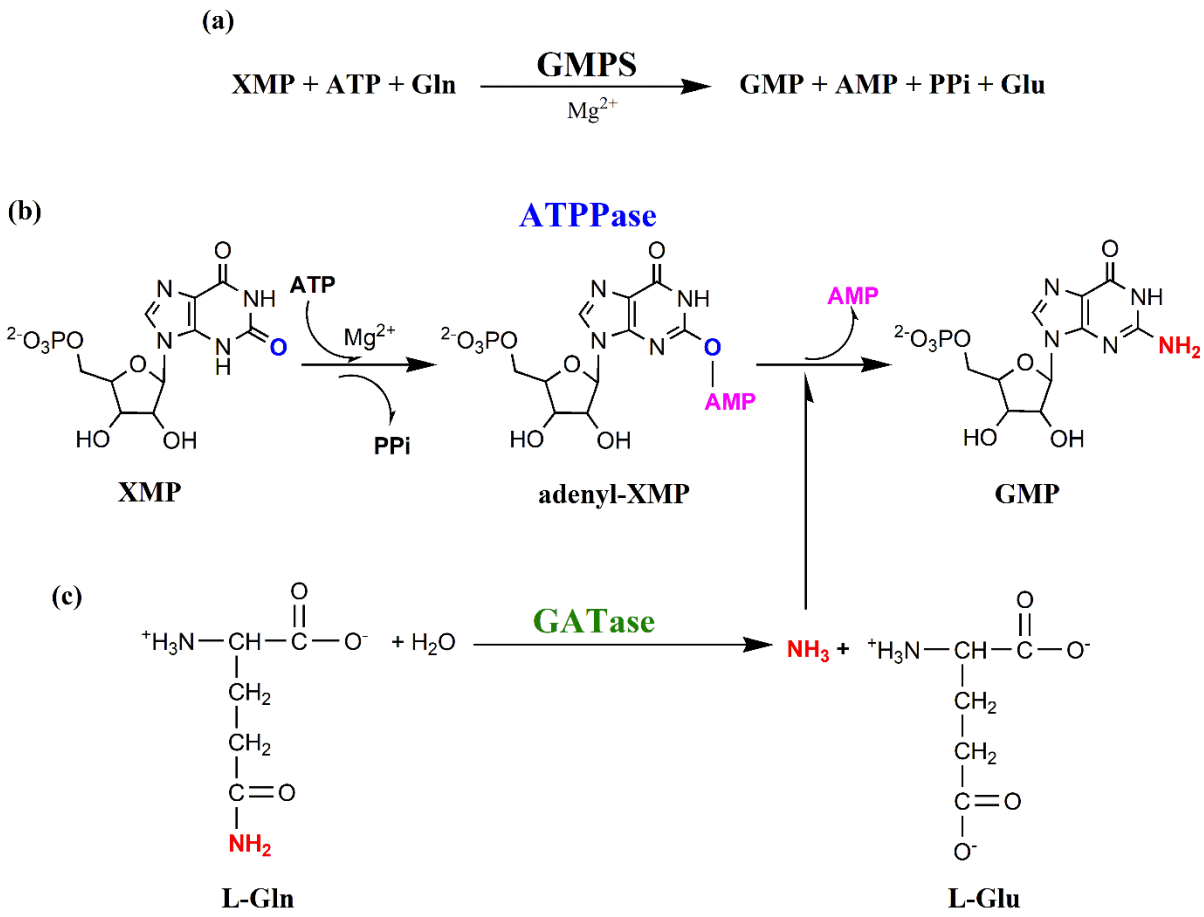
(a)
XMP + ATP + Gln
GMPS
Mg2+
GMP + AMP + PPi + Glu
(b)
ATPPase
ATP
Mg2+
PPi
AMP
AMP
XMP
adenyl-XMP
GMP
(c)
GATase
+ H2O
NH3 +
L-Gln
L-Glu

Figure 2

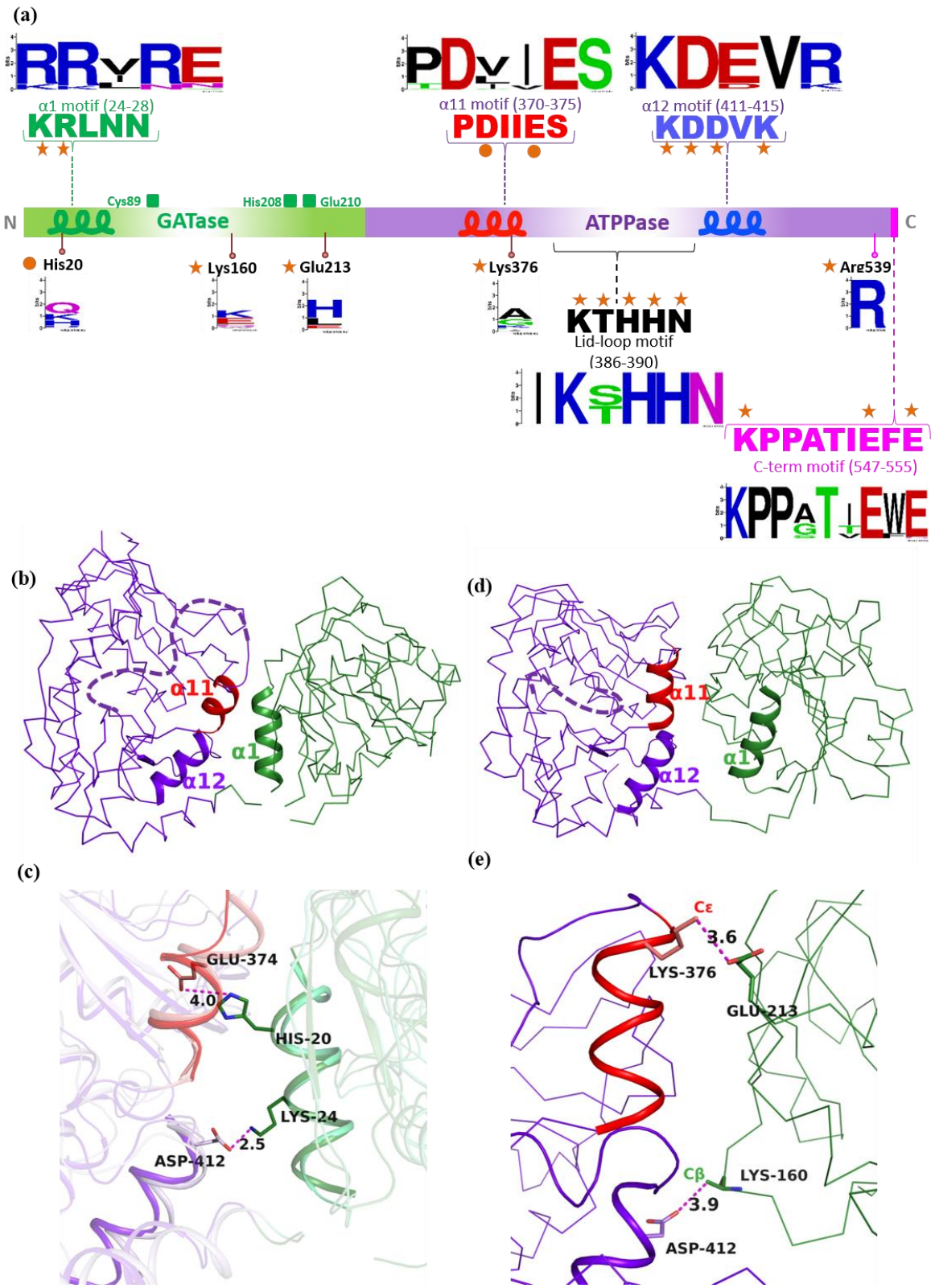
(a)
α1 motif (24-28)
KRLNN
α11 motif (370-375)
PDIIES
α12 motif (411-415)
KDDVK
Cys89
His208
Glu210
N
GATase
ATPPase
C
His20
Lys160
Glu213
Lys376
Arg539
KTHHN
Lid-loop motif
(386-390)
KPPATIEFE
C-term motif (547-555)
(b)
α11
α1
α12
(d)
α11
α1
α12
(c)
GLU-374
4.0
HIS-20
LYS-24
2.5
ASP-412
(e)
Cε
3.6
LYS-376
GLU-213
Cβ
LYS-160
3.9
ASP-412

Figure 3

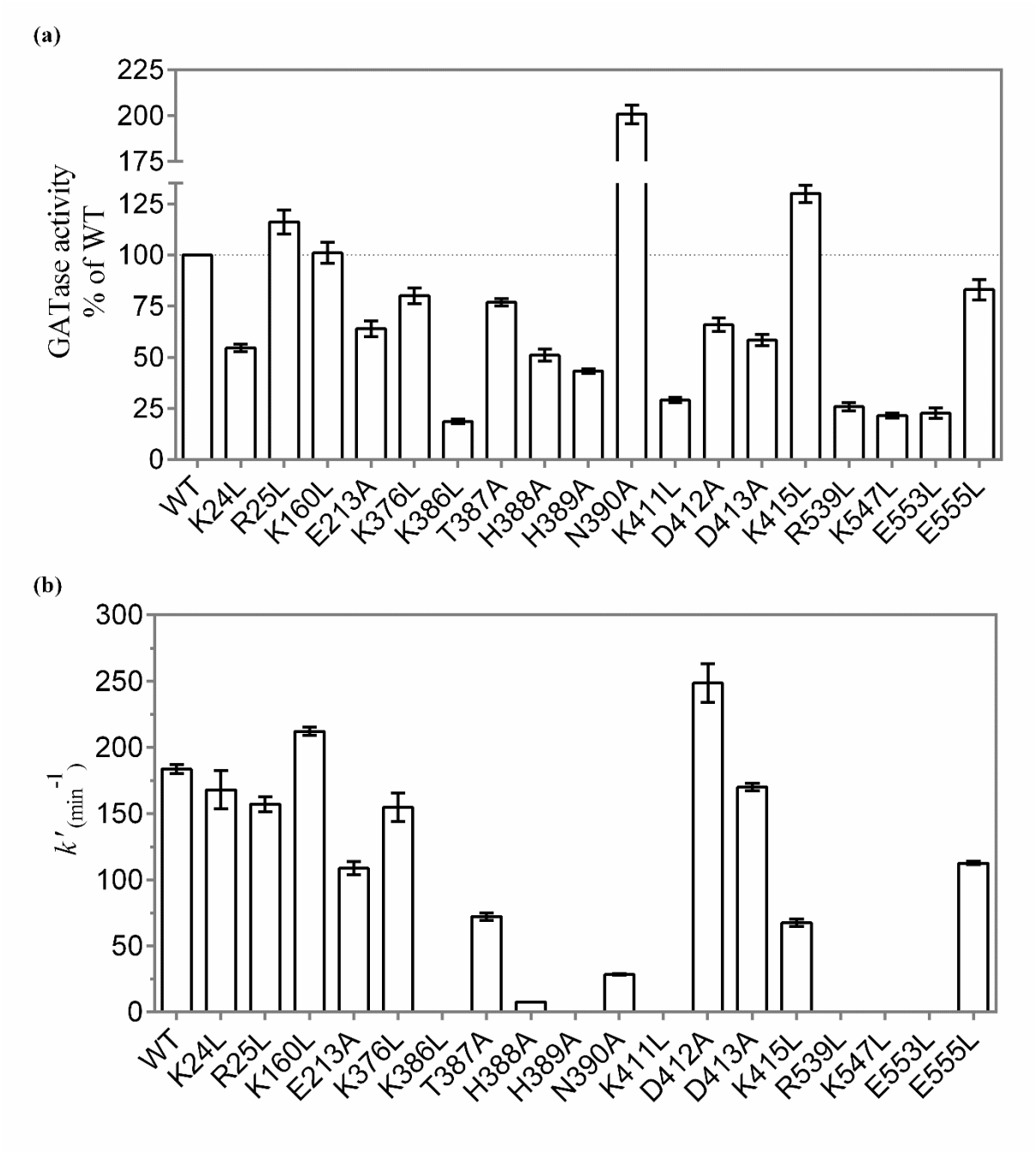
(a)
GATase activity
% of WT
225
200
175
125
100
75
50
25
0
WT
K24L
R25L
K160L
E213A
K376L
K386L
T387A
H388A
H389A
N390A
K411L
D412A
D413A
K415L
R539L
K547L
E553L
E555L
(b)
k′ (min-1)
300
250
200
150
100
50
0
WT
K24L
R25L
K160L
E213A
K376L
K386L
T387A
H388A
H389A
N390A
K411L
D412A
D413A
K415L
R539L
K547L
E553L
E555L

Figure 4

(a)

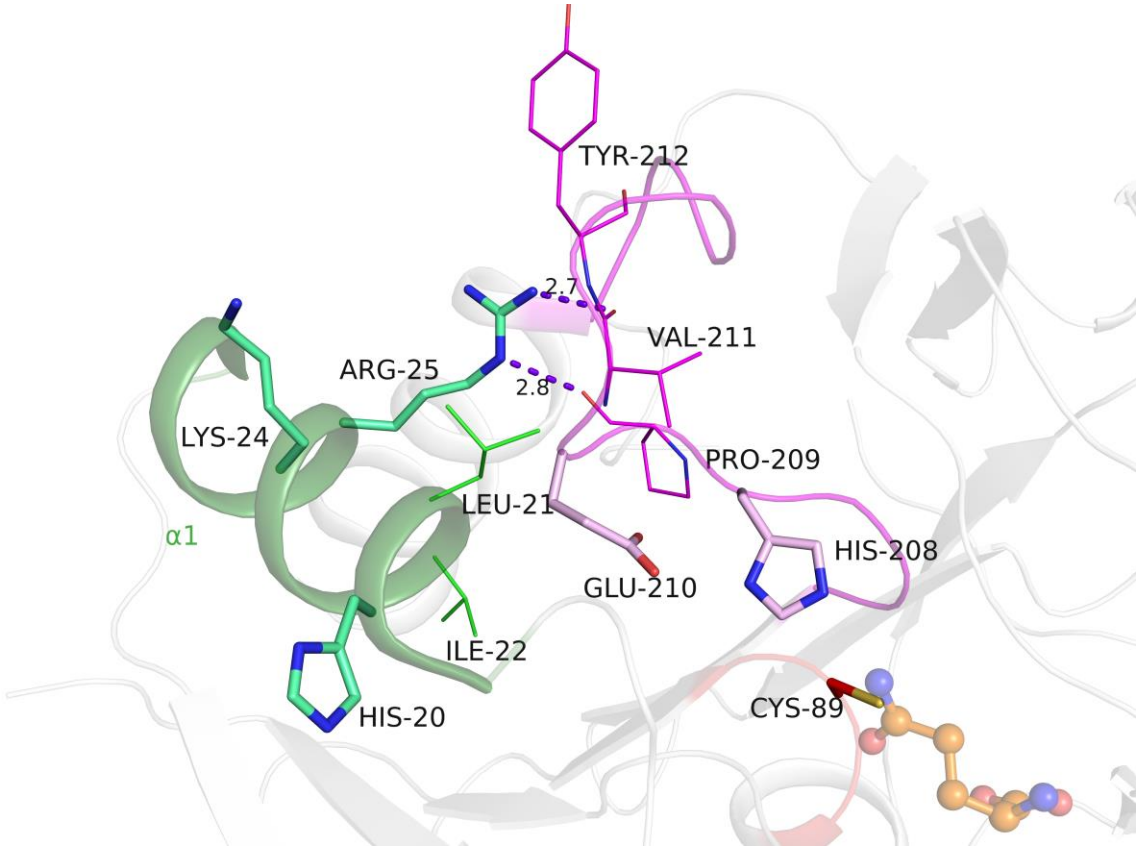
TYR-212
2.7
VAL-211
ARG-25
2.8
LYS-24
PRO-209
LEU-21
α1
HIS-208
GLU-210
ILE-22
HIS-20
CYS-89

(b)

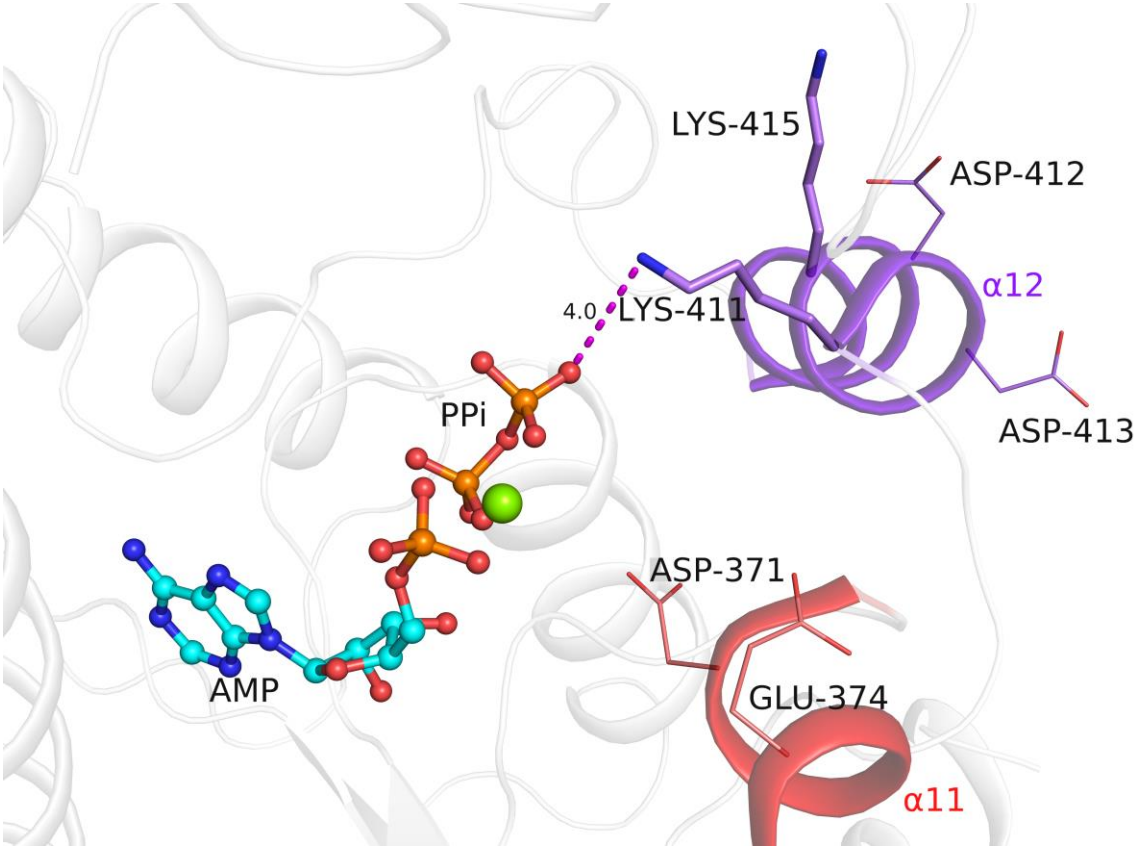
LYS-415
ASP-412
α12
4.0
LYS-411
PPi
ASP-413
ASP-371
AMP
GLU-374
α11

Figure 5

(a)

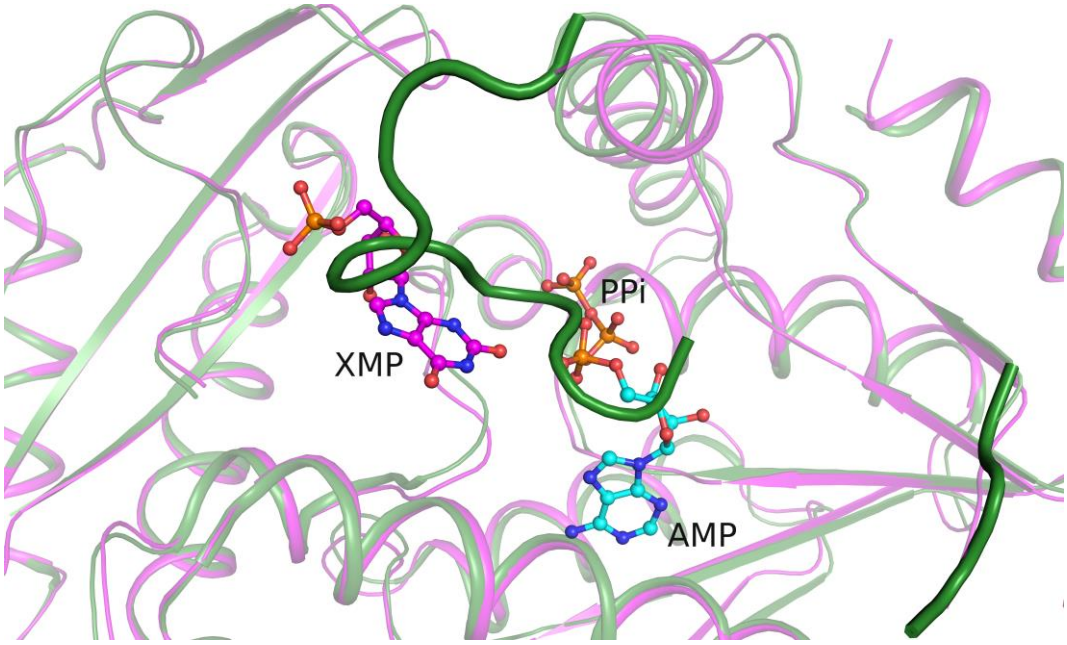
XMP
PPi
AMP

(b)

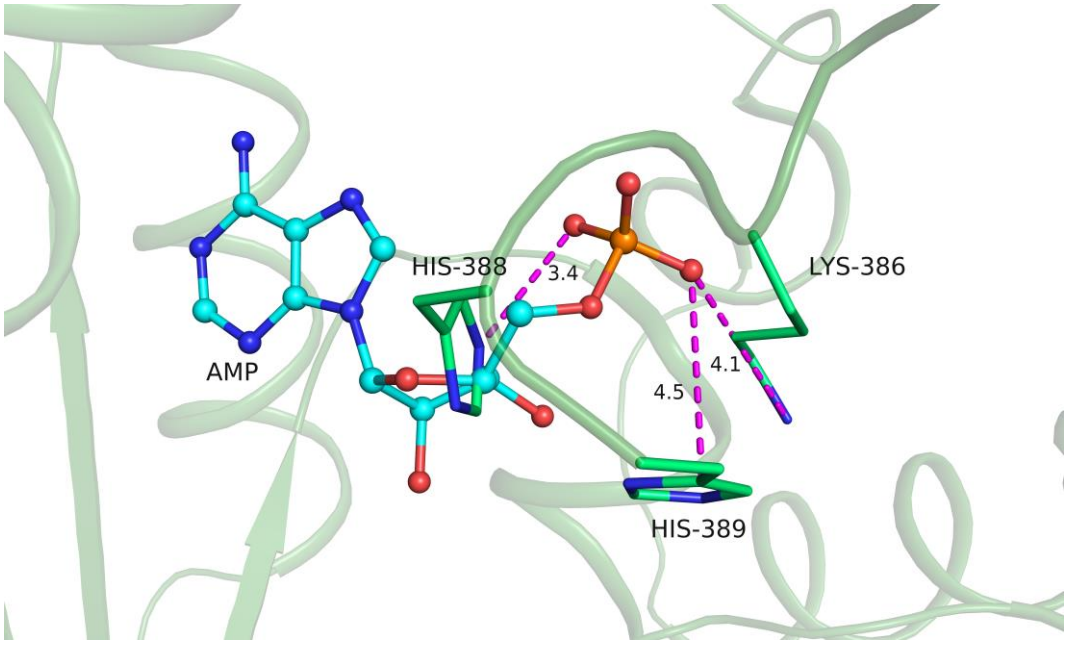
AMP
HIS-388
3.4
LYS-386
4.1
4.5
HIS-389

(c)

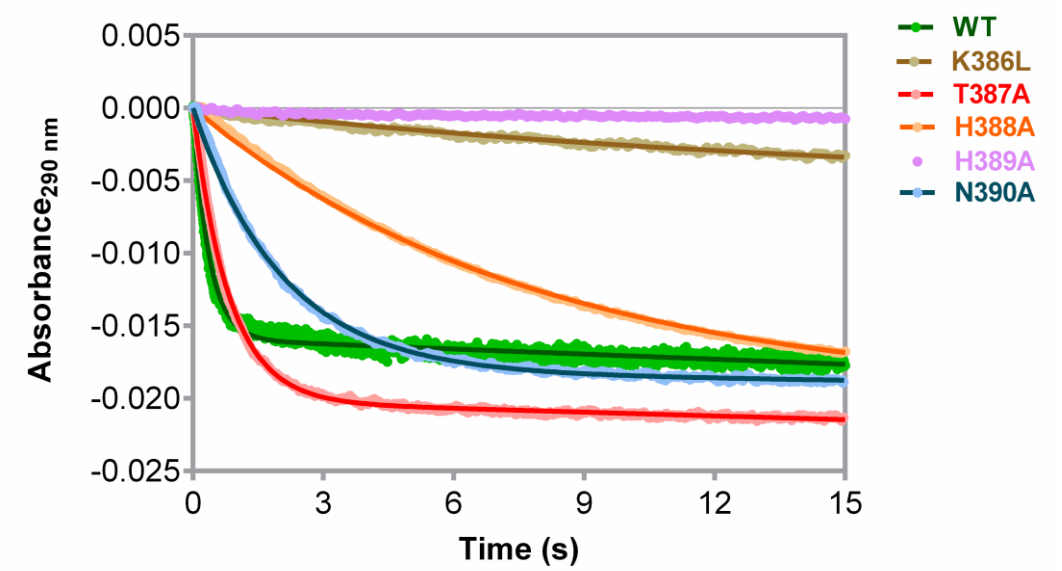
0.005
0.000
-0.005
-0.010
-0.015
-0.020
-0.025
Absorbance290 nm
0
3
6
9
12
15
Time (s)
WT
K386L
T387A
H388A
H389A
N390A

Figure 6

(a)

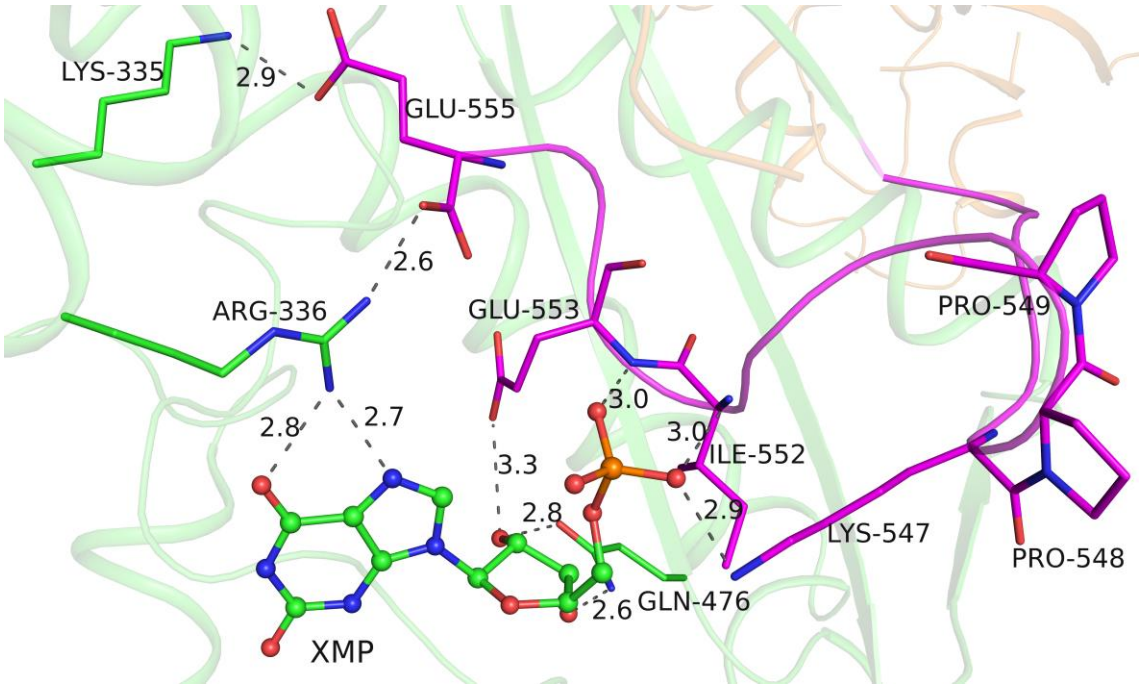
LYS-335
2.9
GLU-555
2.6
ARG-336
GLU-553
PRO-549
3.0
3.0
ILE-552
2.8
2.7
3.3
2.8
2.9
LYS-547
PRO-548
2.6
GLN-476
XMP

(b)

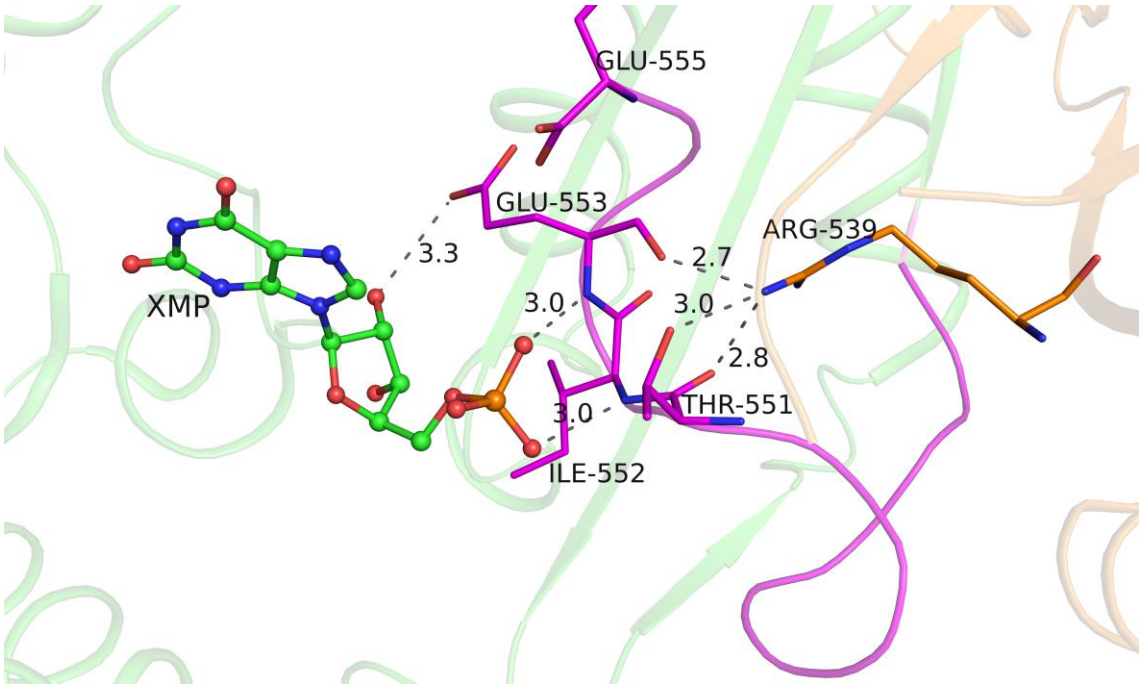
GLU-555
GLU-553
ARG-539
3.3
2.7
XMP
3.0
3.0
2.8
3.0
THR-551
ILE-552

Figure 7

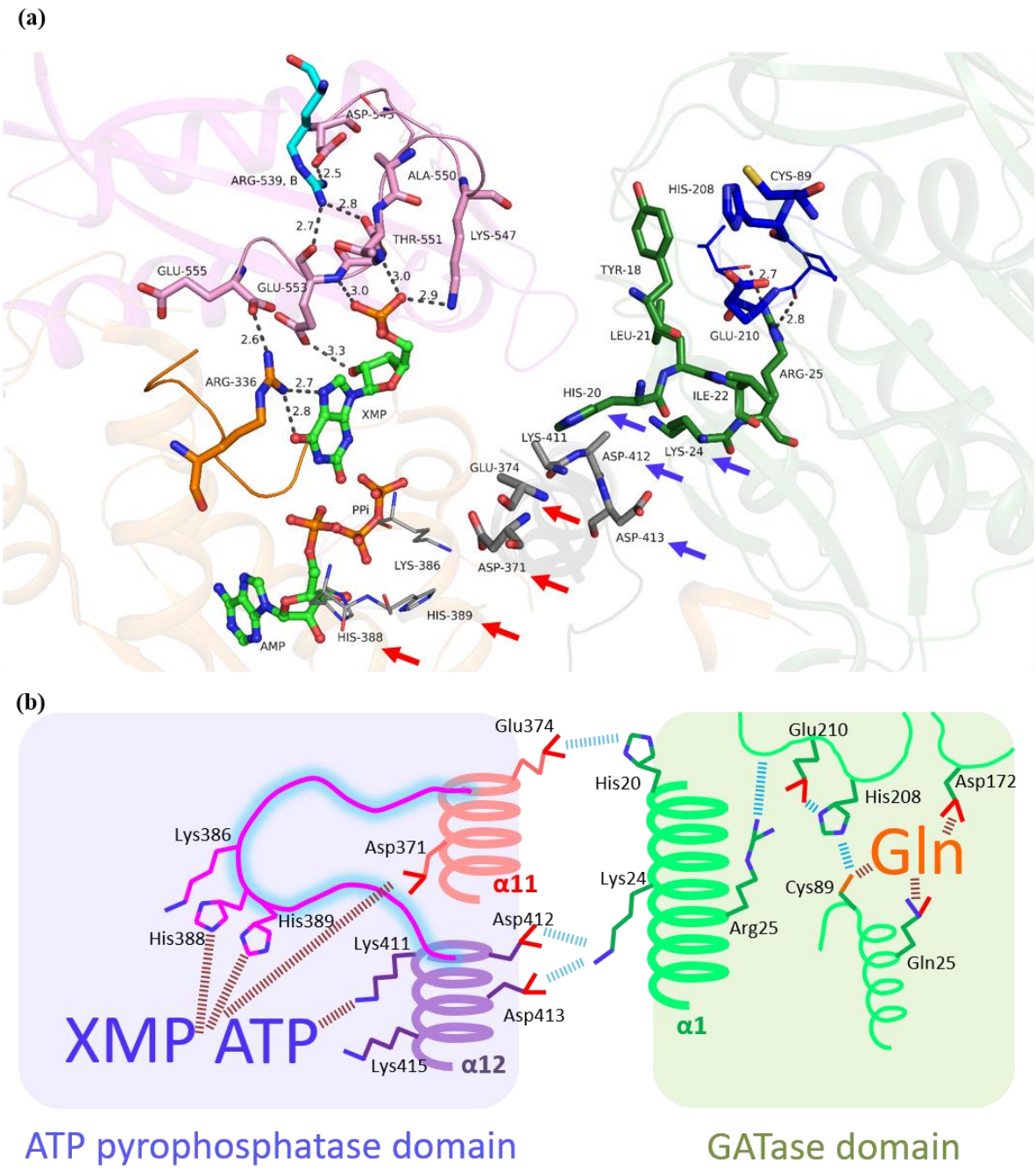
(a)
ARG-539, B
ALA-550
THR-551
LYS-547
GLU-555
GLU-553
ARG-336
XMP
PPi
LYS-386
HIS-389
HIS-388
AMP
HIS-208
CYS-89
TYR-18
LEU-21
GLU-210
ARG-25
HIS-20
ILE-22
LYS-411
ASP-412
LYS-24
GLU-374
ASP-413
ASP-371
(b)
Glu374
Glu210
His20
His208
Asp172
Lys386
Asp371
α11
Lys24
Gln
Cys89
His389
Asp412
Arg25
His388
Lys411
Gln25
Asp413
α1
XMP ATP
Lys415
α12
ATP pyrophosphatase domain
GATase domain

Figure 8

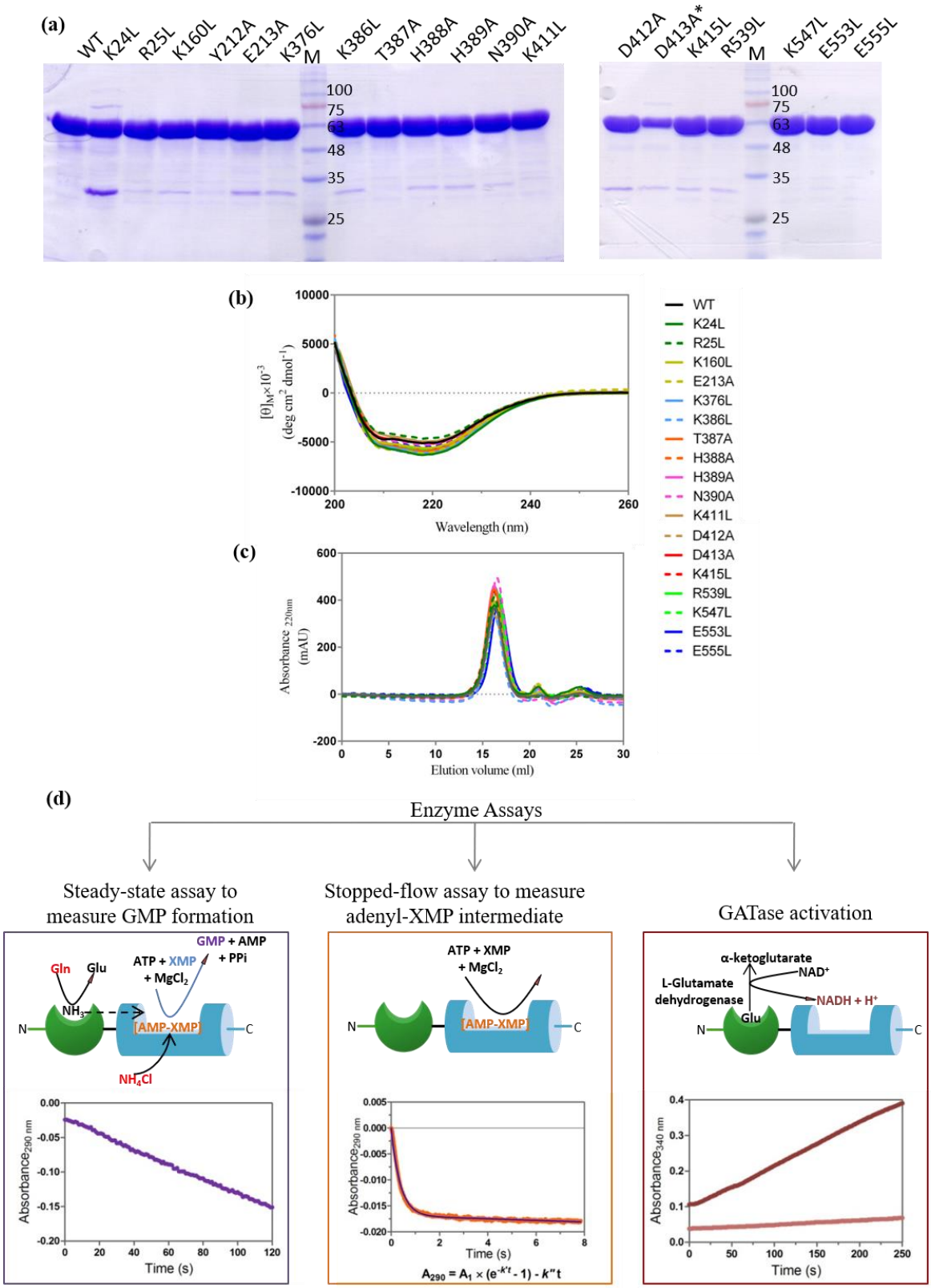
(a)
WT
K24L
R25L
K160L
Y212A
E213A
K376L
M
K386L
T387A
H388A
H389A
N390A
K411L
D412A
D413A*
K415L
R539L
M
K547L
E553L
E555L
100
75
63
48
35
25
(b)
Wavelength (nm)
(c)
Elution volume (ml)
WT
K24L
R25L
K160L
E213A
K376L
K386L
T387A
H388A
H389A
N390A
K411L
D412A
D413A
K415L
R539L
K547L
E553L
E555L
(d)
Enzyme Assays
Steady-state assay to measure GMP formation
Stopped-flow assay to measure adenyl-XMP intermediate
GATase activation
Gln
Glu
ATP + XMP + MgCl2
GMP + AMP + PPi
NH3
[AMP-XMP]
NH4Cl
N
C
Time (s)
ATP + XMP + MgCl2
α-ketoglutarate
NAD+
NADH + H+
L-Glutamate dehydrogenase
Glu
A290 = A1 × (e-k't - 1) - k''t

Figure S1

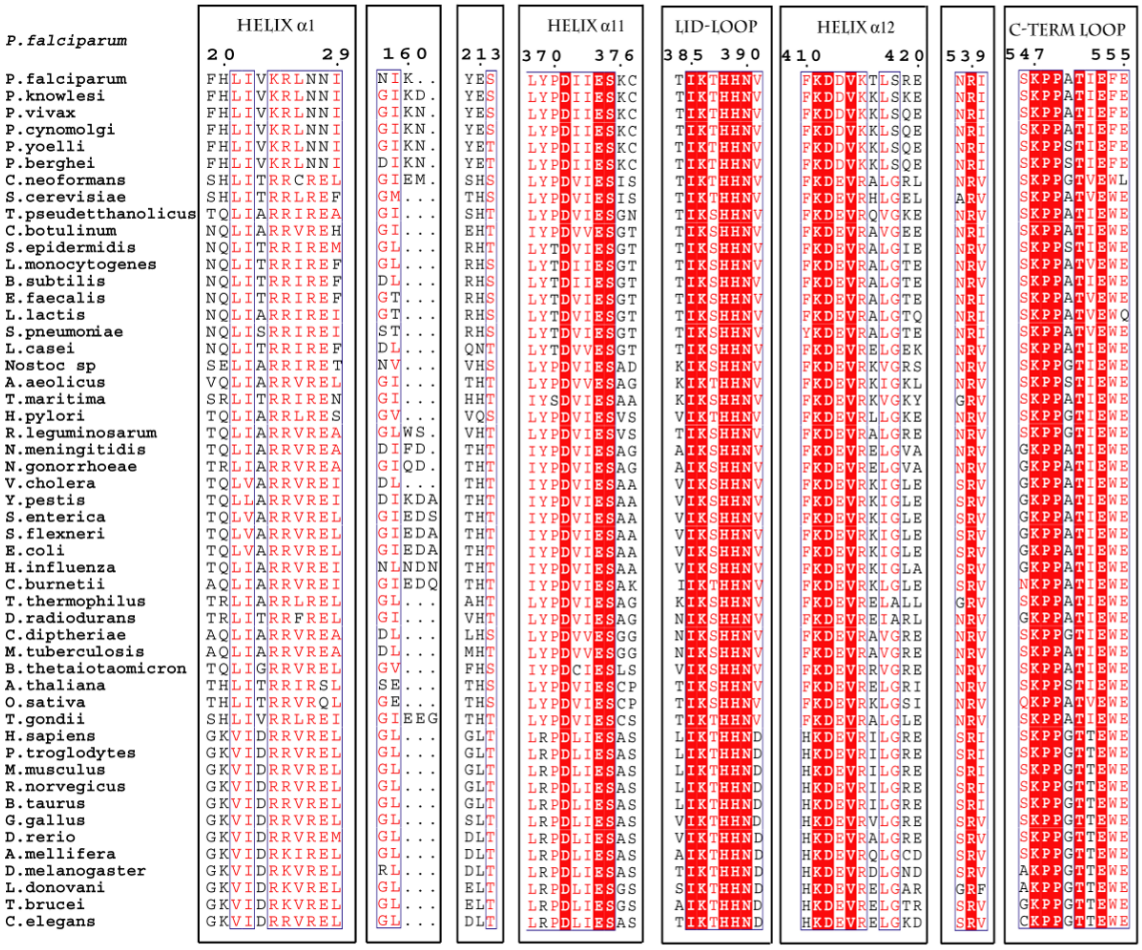
P.falciparum
HELIX α1
HELIX α11
LID-LOOP
HELIX α12
C-TERM LOOP
P.falciparum
P.knowlesi
P.vivax
P.cynomolgi
P.yoelli
P.berghei
C.neoformans
S.cerevisiae
T.pseudetthanolicus
C.botulinum
S.epidermidis
L.monocytogenes
B.subtilis
E.faecalis
L.lactis
S.pneumoniae
L.casei
Nostoc sp
A.aeolicus
T.maritima
H.pylori
R.leguminosarum
N.meningitidis
N.gonorrhoeae
V.cholera
Y.pestis
S.enterica
S.flexneri
E.coli
H.influenza
C.burnetii
T.thermophilus
D.radiodurans
C.diptheriae
M.tuberculosis
B.thetaiotaomicron
A.thaliana
O.sativa
T.gondii
H.sapiens
P.troglodytes
M.musculus
R.norvegicus
B.taurus
G.gallus
D.rerio
A.mellifera
D.melanogaster
L.donovani
T.brucei
C.elegans

Figure S2